Climate Dynamics (2005) 24: 23–43
DOI 10.1007/s00382-004-0485-y

**Hans Renssen · Hugues Goosse · Thierry Fichefet
Victor Brovkin · Emmanuelle Driesschaert · Frank Wolk**

Simulating the Holocene climate evolution at northern high latitudes using a coupled atmosphere-sea ice-ocean-vegetation model

Received: 23 March 2004 / Accepted: 10 September 2004 / Published online: 9 December 2004

Abstract The response of the climate at high northern latitudes to slowly changing external forcings was studied in a 9,000-year long simulation with the coupled atmosphere-sea ice-ocean-vegetation model ECBilt-CLIO-VECODE. Only long-term changes in insolation and atmospheric $CO_2$and CH_4 content were prescribed. The experiment reveals an early optimum (9–8 kyr BP) in most regions, followed by a 1–3°C decrease in mean annual temperatures, a reduction in summer precipitation and an expansion of sea-ice cover. These results are in general agreement with proxy data. Over the continents, the timing of the largest temperature response in summer coincides with the maximum insolation difference, while over the oceans, the maximum response is delayed by a few months due to the thermal inertia of the oceans, placing the strongest cooling in the winter half year. Sea ice is involved in two positive feedbacks (ice-albedo and sea-ice insulation) that lead regionally to an amplification of the thermal response in our model (7°C cooling in Canadian Arctic). In some areas, the tundra-taiga feedback results in intensified cooling during summer, most notably in northern North America. The simulated sea-ice expansion leads in the Nordic Seas to less deep convection and local weakening of the overturning circulation, producing a maximum winter temperature reduction of 7°C. The enhanced interaction between sea ice and deep convection is accompanied by increasing interannual variability, including two marked decadal-scale cooling events. Deep convection intensifies in the Labrador Sea, keeping the overall strength of the thermohaline circulation stable throughout the experiment.

H. Renssen (✉)
Faculty of Earth and Life Sciences,
Vrije Universiteit Amsterdam,
De Boelelaan 1085, 1081 HV, The Netherlands
E-mail: hans.renssen@geo.falw.vu.nl
Tel.: +31-20-4447376
Fax: +31-20-4449940

H. Goosse · T. Fichefet · E. Driesschaert · F. Wolk
Institut d'Astronomie et de Géophysique Georges Lemaître,
Université catholique de Louvain,
Chemin du Cyclotron 2, 1348 Louvain-la-Neuve, Belgium

V. Brovkin
Potsdam Institut für Klimafolgenforschung,
Postfach 601203, 14412 Potsdam, Germany

1 Introduction

Measurements over the last century show evidence of enhanced warming and decreasing sea-ice extent in the Arctic (Folland et al. 2001), which has, for an important part, been associated with anthropogenic forcing (Stott et al. 2000; Mitchell et al. 2001). Indeed, the largest projected future climatic change due to anthropogenic forcing is expected to take place at high latitudes (Cubasch et al. 2001) as an effect of the polar amplification of the warming, involving the ice-albedo positive feedback (e.g., Holland and Bitz 2003). However, projections of future change are hampered by our limited understanding of the natural climate variability, especially on relatively long (centennial–millennial) timescales. In this context, it is important to study the climate evolution at northern high latitudes during the Holocene (i.e. last 11.5 kyr BP, calendar years before the present).

Numerous proxy records from different environments (e.g., glacial, marine, lacustrine, terrestrial) provide valuable information on the Holocene climate evolution at northern high latitudes (e.g., CAPE Project members 2001). However, it is difficult to get a coherent view of Holocene climate change because of the differences between the various records (e.g., Williams and Bradley 1985; Bradley 1990), although recent data syntheses have improved our understanding of this point (Bigelow et al. 2003; Kaufman et al. 2004). Most proxy data give evidence of a thermal optimum early in the Holocene

(10–8 kyr BP, e.g., Ritchie et al. 1983; Bradley 1990; Koerner and Fisher 1990; Koç et al. 1996; Vardy et al. 1998; MacDonald et al. 2000; Snyder et al. 2000; Andreev et al. 2001; Duplessy et al. 2001; Marchal et al. 2002; Kaufman et al. 2004). The timing of this optimum is thought to be a slightly delayed response to the orbitally forced maximum difference (compared to the present) in summer insolation at 11 kyr BP (Berger 1978; Koç and Jansen 1994), i.e. just after the start of the Holocene. Indeed, this difference in insolation is substantial, amounting in June to 39 W/m^2 at 60°N (Berger 1978). However, other proxy data from northern high latitudes indicate that the thermal optimum occurred substantially later (7–4 kyr BP, e.g., Williams and Bradley 1985; Bradley 1990; Korhola et al. 2000; Levac et al. 2001; Kaplan et al. 2002; Smith 2002; Kaufman et al. 2004), probably under the influence of regionally changing environmental conditions, such as the presence of melting ice sheets in the vicinity, or changes in vegetation. In addition, many records give evidence of climate variability superimposed on the long-term trend, showing the occurrence of cooling events at a millennial-to-centennial timescale (e.g., Dahl and Nesje 1996; Korhola et al. 2000; Duplessy et al. 2001; Voronina et al. 2001). It is, however, not clear if these cooling events are synchronous throughout the circumpolar region.

Numerical climate model simulations may be used to improve our understanding of the mechanism behind these Holocene climatic changes and to provide a coherent and physically consistent overview of the climate on all timescales. Climate model studies suggest that orbitally forced changes in insolation are the major factor causing long-term climate variations in the Holocene (e.g., Mitchell et al. 1988; Kutzbach and Gallimore 1988; Hewitt and Mitchell 1998; Braconnot et al. 2000; Weber 2001; Crucifix et al. 2002; Brovkin et al. 2002; Weber and Oerlemans 2003; Weber et al. 2004). In addition, internal feedbacks play a role, of which sea ice-albedo and taiga-tundra feedbacks are the most important, as they significantly modify the surface albedo (e.g., Kerwin et al. 1999; Harvey 1988; Foley et al. 1994). Although a wealth of information is obtained in these model studies, an important limitation is that most studies only consider the climate in equilibrium with 9 or 6 kyr BP boundary conditions. It is, however, uncertain if the climate system was really in equilibrium at these times, given the constantly changing orbital forcing and the slow disintegration of ice sheets in the early Holocene, and the possible non-linear interactions between climatic sub-systems in response to these changes (e.g., Claussen et al. 1999; Brovkin et al. 2003; Renssen et al. 2003a). Ideally, therefore, the climate system's transient response to forcings is accounted for in Holocene modeling studies.

Recently, several groups (Weber 2001; Crucifix et al. 2002; Brovkin et al. 2002; Wang et al. 2004) have simulated the Holocene climate evolution with earth system models of intermediate complexity (EMICs, Claussen et al. 2002). These studies show that all compartments of the coupled system actively participate and interact during the Holocene. However, the models applied by Crucifix et al. (2002), Brovkin et al. (2002) and Wang et al. (2004) have a relatively coarse resolution and include highly simplified representations of the atmosphere. The model of Weber (2001) includes a more comprehensive atmospheric module that simulates synoptic variability, but contains a simplified ocean component (viz., with flat bottom topography and T21 resolution, and without sea-ice advection) and lacks a dynamic vegetation model. As a consequence of these model limitations, transient Holocene experiments have so far not been used for a detailed analysis of the spatial patterns of change during the Holocene or for a study of the influence of atmospheric and oceanic circulation changes at a centennial–millennial timescale.

To improve our understanding of the spatial and temporal climate variability during the Holocene, we have therefore applied a 3-dimensional global atmosphere-sea ice-ocean-vegetation model (described in Sect. 2) to simulate the Holocene climate evolution of the last 9 kyr. In our experiment, we have only prescribed the changing insolation and the long-term changes in the atmospheric CH_4 and CO_2 content. We also discuss here the results of a sensitivity experiment in which we investigate the effect of the residual Laurentide Ice Sheet on the early Holocene climate. Our main objective is to estimate the part of the Holocene climate variability observed in different areas of the northern high latitudes (i.e. north of 60°N) that could be explained by a response of the coupled climate system to slowly changing external forcings. To our knowledge, this is the first transient Holocene simulation of the Artic climate with a coupled 3-dimensional climate model including a dynamic vegetation component that resolves synoptic variability associated with weather patterns. In Sect. 3, we first present our simulation results, thereby focusing on selected regions for which sufficient proxy data are available for a model-data comparison (i.e. Scandinavia, Greenland, Northern North America and Northern Eurasia, Fig. 1). The model results are then compared with available proxy records in Sect. 4. In Sect. 5, we analyze the mechanisms responsible for the climate changes during the Holocene, followed by concluding remarks.

2 Methods

2.1 Model

We have performed our numerical experiment with the ECBilt-CLIO-VECODE model (version 3) that describes the dynamics of the atmosphere-sea ice-ocean-vegetation system. The atmospheric component of this global, 3-dimensional model is version 2 of ECBilt, a spectral T21, three-level, quasi-geostrophic model developed at the Koninklijk Nederlands Meteorologisch Instituut (KNMI) (Opsteegh et al. 1998). ECBilt in-

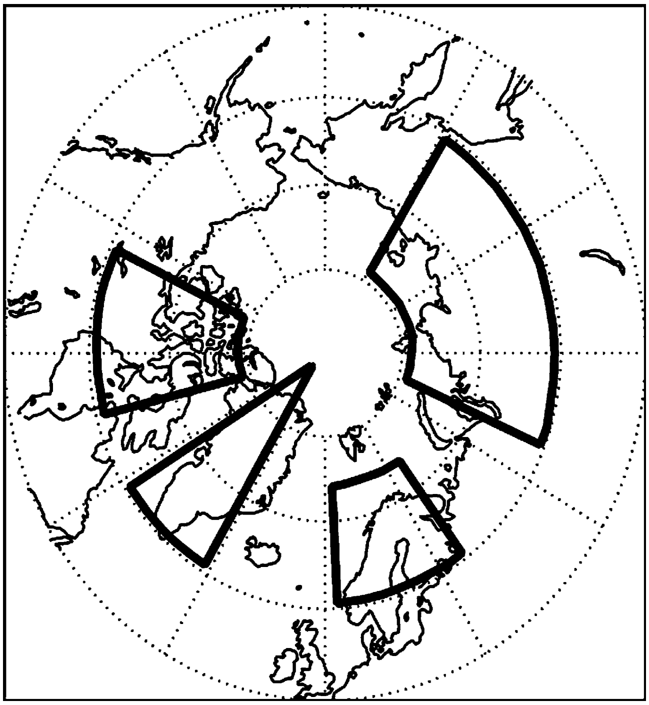

Fig. 1 Map showing the regions north of 60°N for which the long-term Holocene climate evolution is studied: Scandinavia, northern North America, Greenland and Northern Eurasia

cludes a representation of the hydrological cycle and simple parameterizations of the diabatic heating processes. Cloudiness is prescribed according to present-day climatology (Rossow et al. 1996) and a dynamically passive stratospheric layer is included. As an extension to the quasi-geostrophic equations, an estimate of the neglected terms in the vorticity and thermodynamic equations is incorporated as a temporally and spatially varying forcing (Opsteegh et al. 1998). This forcing is computed from the diagnostically derived vertical motion field. With these ageostrophic terms, the simulation of the Hadley circulation is considerably improved, resulting in a drastic improvement of the strength and position of the jet stream and transient eddy activity. The hydrological cycle is closed over land by using a bucket for soil moisture. Each bucket is connected to a nearby oceanic grid cell to define river runoff. Accumulation of snow occurs in case of precipitation in areas with below 0°C surface temperature.

The sea ice-ocean component is the CLIO model built at Université catholique de Louvain (Goosse and Fichefet 1999). CLIO consists of a primitive-equation, free-surface ocean general circulation model (OGCM) (Deleersnijder and Campin 1995; Campin and Goosse 1999), coupled to a comprehensive thermodynamic–dynamic sea-ice model (Fichefet and Morales Maqueda 1997). The OGCM includes a detailed formulation of boundary layer mixing based on Mellor and Yamada's (1982) level-2.5 turbulence closure scheme (Goosse et al. 1999) and a parameterization of density-driven downslope flows (Campin and Goosse 1999). The sea-ice model takes into account the heat capacity of the snow-ice system, the storage of latent heat in brine pockets trapped inside the ice, the effect of the subgrid-scale snow and ice thickness distributions on sea-ice thermodynamics, the formation of snow ice under excessive snow loading and the existence of leads within the ice cover. Ice dynamics are calculated by assuming that sea ice behaves as a 2-dimensional viscous-plastic continuum. The horizontal resolution of CLIO is 3° latitude by 3° longitude, and there are 20 unequally spaced vertical levels in the ocean.

The model applied is an updated and improved version of the model used earlier for a variety of applications, i.e. to simulate the present-day climate (Goosse et al. 2001; 2003), to study freshwater-induced abrupt climate events during the early Holocene (Renssen et al. 2001, 2002), natural variability of the modern climate (Goosse et al. 2002a) and future climate evolution (Goosse and Renssen 2001; Schaeffer et al. 2002). Compared to this earlier version, the present model simulates a climate that is closer to modern observations. The most important improvements in the new version are a new land surface scheme that takes into account the heat capacity of the soil, and the use of isopycnal diffusion as well as Gent and McWilliams parameterization to represent the effect of meso-scale eddies in the ocean (Gent and McWilliams 1990). The climate sensitivity of ECBilt-CLIO is about 0.5°C/(W/m^2), which is at the lower end of the range (typically 0.5–1°C/(W/m^2)) found in most coupled climate models (Cubasch et al. 2001). The only flux correction required in ECBilt-CLIO is an artificial reduction of precipitation over the Atlantic and Arctic Oceans, and a homogeneous distribution of the removed amount of freshwater over the Pacific Ocean (Goosse et al. 2001).

ECBilt-CLIO has recently been coupled to VECODE, a dynamic global vegetation model developed at the Potsdam Institut für Klimafolgenforschung (PIK, Brovkin et al. 2002). VECODE simulates dynamics of two main terrestrial plant functional types, trees and grasses, as well as desert (bare soil), in response to climate change. Within ECBilt-CLIO-VECODE, simulated vegetation changes affect only the land-surface albedo, and have no influence on other processes, e.g., evapotranspiration. VECODE does not simulate plant types that are specific for the Arctic region (dwarf shrubs, forbs, mosses, etc.), but uses a bulk approach of representing vegetation cover as a mixture of trees and herbaceous plants. This simplification is common for the global dynamic vegetation models (Cramer et al. 2001). In the Arctic region, distinguishing of trees from the other plants allows us to capture a first-order effect of vegetation on climate since trees are taller than snow cover and their presence modifies radiative budget at the surface during the snow season. The ECBilt-CLIO-VECODE model has been applied to study the long-term effect of global deforestation on climate (Renssen et al. 2003b). It should be noted that our model has only the atmospheric component ECBilt in common with the model version used by Weber (2001) and Weber and Oerlemans (2003), as they used a version with a flat-bottom ocean model without sea-ice dynamics at lower resolution (T21) and with no dynamic vegetation component.

2.2 Experimental design

To simulate the climate evolution of the last 9 kyr, we have forced the ECBilt-CLIO-VECODE model by annually varying insolation (Berger 1978) and long-term trends (i.e. without high-frequency variations) of the atmospheric concentrations of CO_2 and CH_4 (Raynaud et al. 2000) for the 9–0 kyr BP period (Fig. 2). At 60°N, the June insolation is reduced by 39 W/m^2 (i.e. 7.7%) over the last 9 kyr (Fig. 2a). The annual insolation decreases slightly by 2 W/m^2, while during the winter half year (September–March) it increases (i.e. 12 W/m^2, maximum difference of +27 W/m^2 in October). The atmospheric CH_4 content decreases by about 70 ppbv until 5 kyr BP, but rises again by 130 ppbv during the last 4.5 kyr (Fig. 2b). The increase in atmospheric CO_2 content is about 20 ppmv in 9 kyr. We fixed all other forcings (i.e. other greenhouse gas concentrations, solar constant) at their preindustrial values (i.e. 1750 AD). The initial conditions were obtained from an experiment that was run until equilibrium with 9 kyr BP insolation and trace gas concentrations. It should be noted that we did not take the effect of high frequency changes in forcings into account, of which the most important ones are the changes in solar and volcanic forcing. For the last millennium, the effect of these forcings has been studied in experiments performed with an earlier model version (Goosse et al. 2004; Goosse and Renssen 2003, 2004).

The experiment was started at 9 kyr BP because our model lacks a dynamical ice-sheet model that could simulate the deglaciation of the Laurentide and Scandinavian Ice Sheets earlier in the Holocene. We realize that the final disintegration of the Laurentide Ice Sheet was not completed before ~7 kyr BP (Peltier 1994). Regrettably, with the present model setup it is not feasible to perform a full deglaciation experiment, as this would require a dynamic ice-sheet component. Nevertheless, to estimate the first-order effect of the residual Laurentide Ice Sheet on climate, we performed an additional, highly idealized experiment for the period 9–6 kyr BP (hereafter called ICE) in which we prescribed identical forcings as in the main simulation (hereafter MAIN), but with an additional, static Laurentide Ice Sheet between 9 and 7 kyr BP that was removed instantaneously at 7 kyr BP. For this ice sheet, the 8.5 kyr BP characteristics (altitude and extent) were

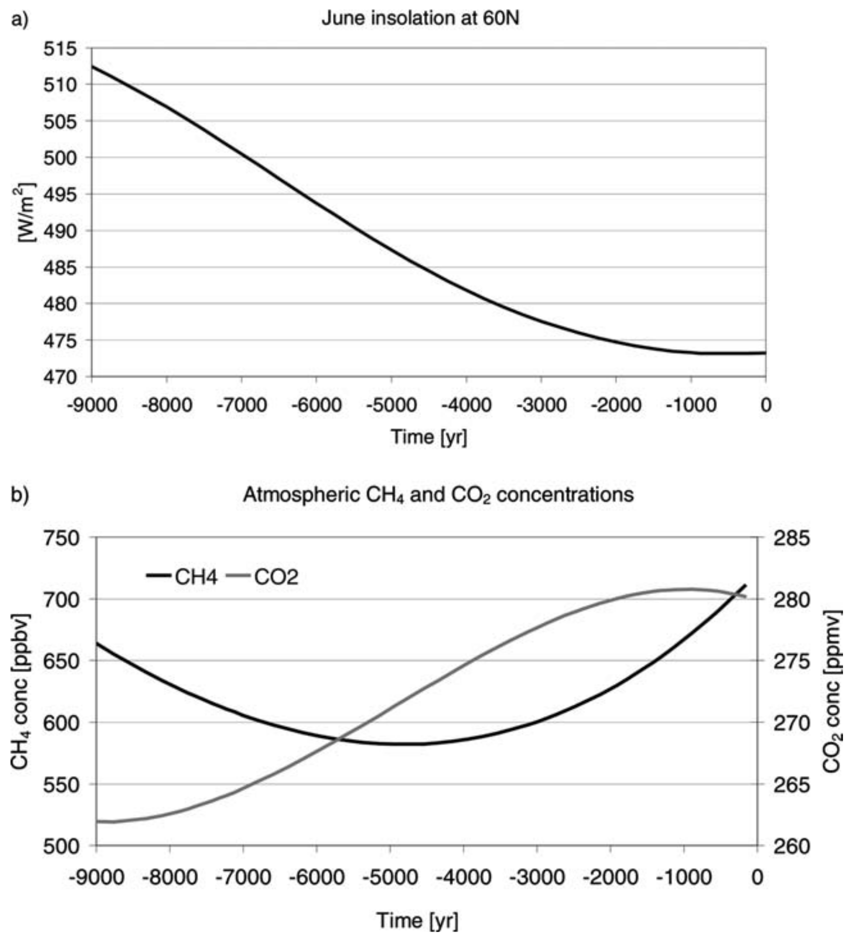

Fig. 2 Time-series of forcings prescribed in the experiment. **a** Insolation (W/m^2) at 60°N (Berger 1978), and **b** smoothed atmospheric concentrations of CH_4 and CO_2. The latter curves are obtained by fitting a 3rd order polynomial function through the ice core data presented in Raynaud et al. (2000)

chosen, i.e. without a dome over the Hudson Bay (Peltier 1994). In ICE, the melt water runoff due to the ice sheet melting is not taken into account.

In this paper, the results are presented as deviations from the preindustrial mean, for which we have taken the period 1,000–250 years BP (i.e. 1000–1750 AD). We focus on the model results that can be compared with proxy data, i.e. surface temperatures, precipitation, sea-ice conditions and vegetation response.

3 Model results

3.1 Surface temperatures

3.1.1 General

The evolution of the temperatures averaged over the area north of 60°N (Fig. 3a, b) shows a long-term cooling trend in both winter and summer, with a total cooling of about 2°C. The temperature evolution in July follows closely the summer insolation curve (Fig. 3b), whereas the January temperatures remain at about the same level until 6 kyr BP, after which an enhanced cooling phase is noted that lasts until 1 kyr BP (Fig. 3a). Compared to July, the temporal variability is much larger in January, including a phase of distinct multi-centennial temperature fluctuations between 3.5 and 1.5 kyr BP. The results of the ICE experiment suggest that in MAIN the July temperatures are overestimated between 9 and 7 kyr BP (~0.5°C difference), whereas no ice sheet effect is found for the January temperatures.

The mapped 0–9 k temperature anomalies reveal considerable spatial variability, with marked different responses over land and ocean surfaces (Fig. 4a–e). Over the continents, the Holocene temperature decrease is strongest in summer (June–July–August) in line with the insolation forcing, with a maximum cooling of 7°C in the Canadian Arctic (Fig. 4c). Over the oceans, however, the maximum temperature difference lags the continental response by several months. The western part of the Arctic Ocean experiences a maximum cooling of up to 7°C during autumn (September–October–November, Fig. 4d), whereas in the Barents Sea the greatest temperature depression occurs in winter (December–January–February, Fig. 4a). In most regions, the season with the minimum change in temperature is spring (March–April–May, Fig. 4b). In autumn, moderate warming (up to 2°C) is experienced between 60 and 65°N in eastern Siberia, while in western Siberia and Europe a slight increase in temperature is noted in spring. However, on an annual basis, all areas north of 60°N experience a decrease in temperature in the model (Fig. 4e).

3.1.2 Scandinavia

In our experiment, the temperatures in Scandinavia were highest during the first 500 years of the experiment, after which they decrease almost linearly towards the preindustrial climate (Fig. 5a, b and Table 1). According to the model, the total cooling over the last 9 kyr is 1.5°C in July and 2.0°C in January. The latter anomaly is strongly influenced by the strong winter cooling over the Nordic Seas (Greenland-Icelandic-Norwegian Seas, see Fig. 4a), of which a part is included in the calculation of the average depicted in Fig. 5a. In addition, the interannual variability (as expressed by the standard deviations in Table 1) increases considerably, most notably in winter during the last 4 kyr. This increase in variability culminates in several cold excursions that lasts up to a few decades (e.g., around 2.5 and 1.7 kyr BP) and reach 15°C below the long-term January mean.

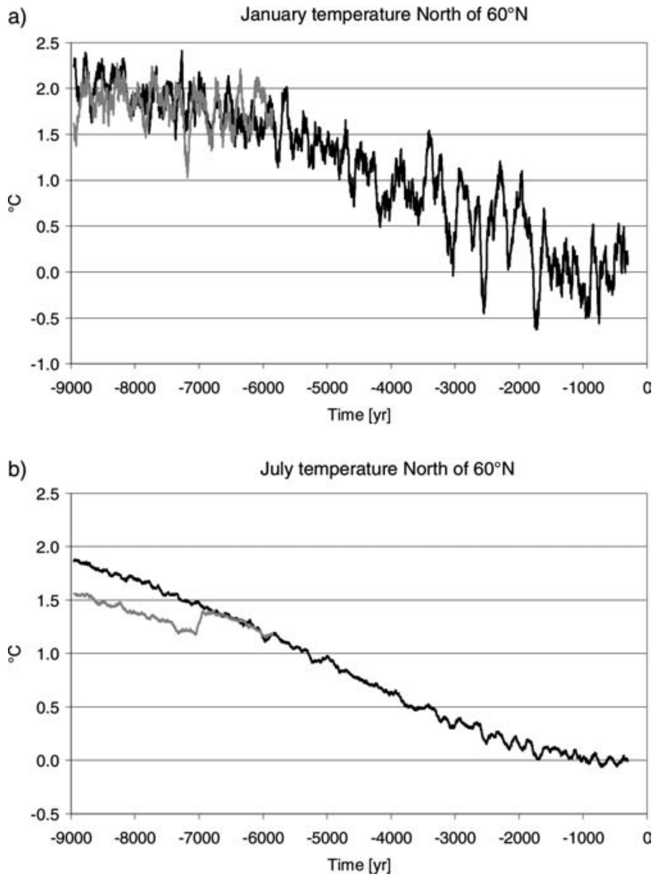

Fig. 3 Simulated time series (100-point running means) of surface temperature (°C) averaged over the area north of 60°N, shown as deviations from the preindustrial mean (1,000–250 yr BP). **a** January, and **b** July. *The black line* represents MAIN, *the gray line* ICE. The preindustrial means for January and July temperatures are −27.5 and 8.8°C, respectively

3.1.3 Northern North America

The long-term temperature trends in northern North America are quite different compared to the trends simulated for northern Europe (Fig. 6a, b). In January, the temperature decrease is smaller in North America (about 1°C), whereas in July the cooling is much more

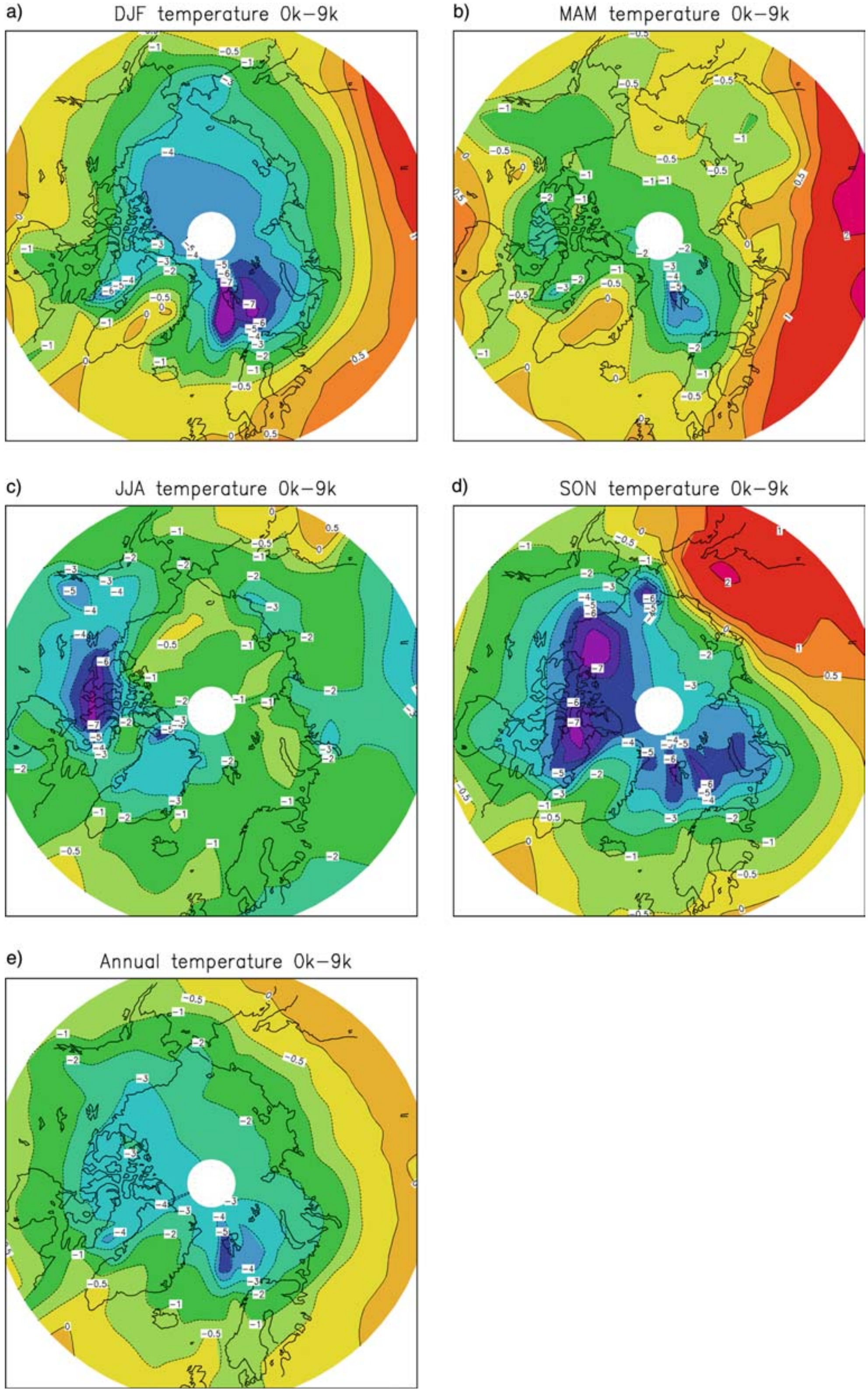

Fig. 4 Simulated seasonal preindustrial minus 9–8 k change in surface temperature (°C). **a**DJF, **b** MAM, **c**JJA, **d** SON, and **e** annual

expressed (more than 5°C). However, in the ICE simulation, the long-term mean July temperature is more than 1°C lower between 9 and 7 kyr BP than in MAIN. Moreover, after the removal of the Laurentide Ice Sheet at 7 kyr BP, the July temperatures in ICE reach mean values that are higher than at 9 kyr BP, suggesting that the residual Laurentide Ice Sheet could have delayed the thermal maximum by a few thousand years. In the July temperature evolution, a marked increase in the interannual variability is noted after 5 kyr BP, which is even

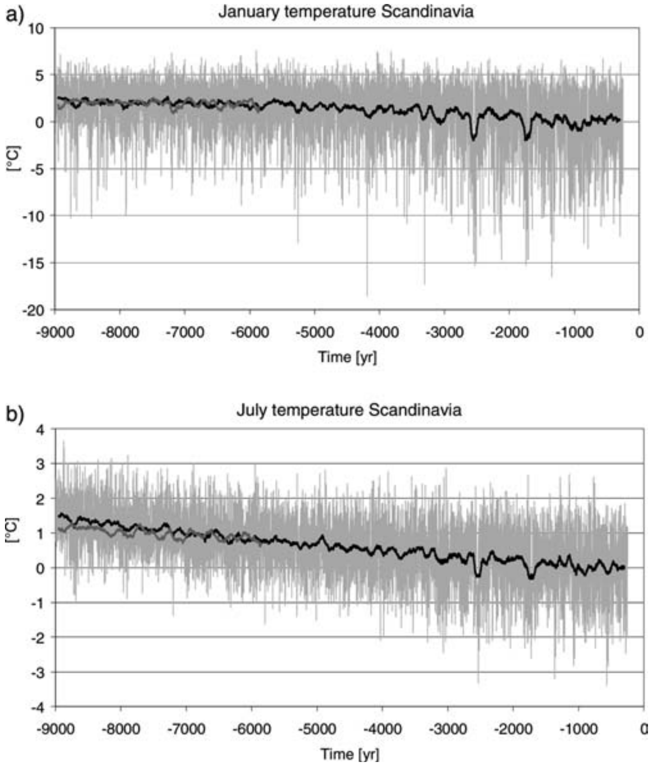

Fig. 5 Simulated surface temperature (°C) evolution for Scandinavia (62–74°N, 8–36°E), shown as deviations from the preindustrial mean (1,000–250 yr BP). **a**January, **b** July. The unfiltered results of MAIN are shown by the *thin gray line*, whereas the *thick lines* represent the 100-point running averages of MAIN (*black*) and ICE (*dark gray*). The preindustrial means for January and July temperatures are −11.3 and 13.1°C, respectively

more expressed than in the result of northern Europe (see Table 1), although no clear decadal-scale cold excursions are noted.

3.1.4 Greenland

The simulated July temperature evolution for Greenland (Fig. 7a, b) shows a response that is intermediate between North America and northern Europe. The July temperature decreases by about 3°C over 9 kyr, but this is probably an overestimation (by about 0.5°C), as the effect of the summer insolation surplus was tempered by the residual Laurentide Ice Sheet in the early Holocene (compare ICE with MAIN in Fig. 7b). In January, only a moderate long-term decrease in temperature is simulated (i.e. less than 1°C). In contrast to North America and northern Europe, no significant increase in temporal variability is found in Greenland (Table 1).

3.1.5 Northern Eurasia

The simulated thermal evolution in northern Eurasia is similar to that of Scandinavia, with a 1.6°C temperature decrease in both January and July (Fig. 8a, b). The

Table 1 Absolute surface temperatures and precipitation in four selected land areas and four time periods: early Holocene (9–7 kyr BP), Mid Holocene (7–4 kyr BP), Late Holocene (4–1 kyr BP) and preindustrial (1,000–250 yr BP)

Simulated variable	Time periods (kyr BP)															
	Scandinavia				N North America				Greenland				N Eurasia			
	9–7	7–4	4–1	Preindustrial	9–7	7–4	4–1	Preindustrial	9–7	7–4	4–1	Preindustrial	9–7	7–4	4–1	Preindustrial
January temperature (°C)	−9.24	−9.65	−10.75	−11.31	−25.76	−26.00	−26.25	−26.59	−22.63	−22.77	−23.11	−23.39	−41.49	−41.80	−42.34	−42.87
SD	2.31	2.52	3.42	3.51	4.13	4.23	4.35	4.46	1.57	1.59	1.63	1.57	3.48	3.61	3.64	3.66
July temperature (°C)	14.37	13.87	13.38	13.14	14.07	12.53	9.85	8.96	1.97	0.73	−0.38	−0.68	17.63	17.17	16.45	16.14
SD	0.66	0.71	0.87	0.90	0.67	1.13	1.48	1.55	0.60	0.67	0.53	0.53	0.62	0.59	0.62	0.63
January precipitation (mm)	41.30	41.32	41.62	41.82	18.46	18.66	18.54	18.71	55.63	56.28	56.61	56.28	23.22	23.69	23.74	23.58
SD	6.30	6.50	6.72	6.73	3.83	3.99	4.09	4.17	8.91	9.39	9.57	9.48	3.96	3.98	3.90	3.71
July precipitation (mm)	45.54	45.36	45.47	45.89	87.88	78.20	66.06	62.92	68.28	63.93	62.88	63.66	79.33	73.79	67.84	65.69
SD	8.69	8.91	8.27	8.28	11.52	11.37	10.19	9.97	5.37	4.68	4.31	4.56	7.54	6.50	5.67	5.62

The monthly standard deviations (SD) are also shown

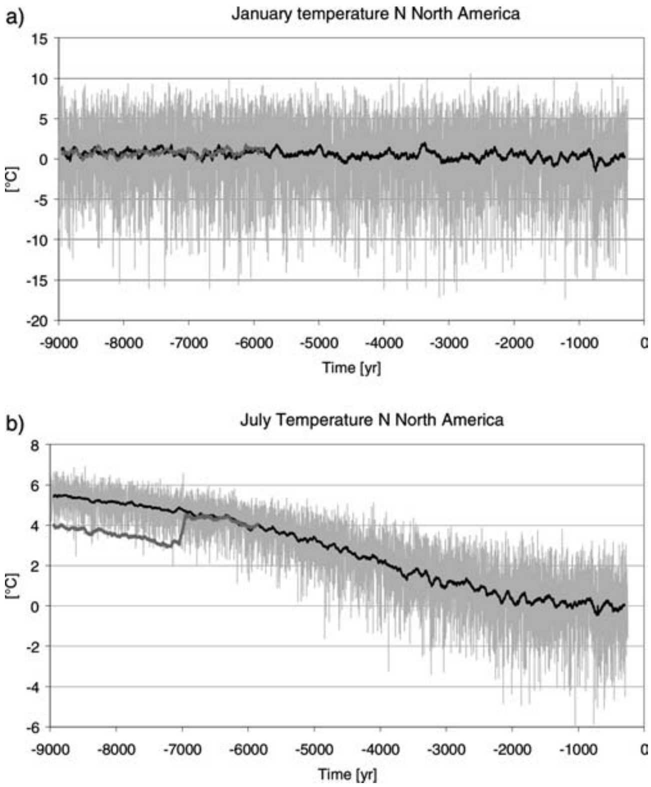

Fig. 6 Simulated surface temperature (°C) evolution for northern North America (62–78°N, 115–76°W), shown as deviations from the preindustrial mean (1,000–250 yr BP). **a** January, **b** July. The unfiltered results of MAIN are shown by the *thin gray line*, whereas the *thick lines*represent the 100-point running averages of MAIN (*black*) and ICE (*dark gray*). The preindustrial means for January and July temperatures are −26.6 and 9.0°C, respectively

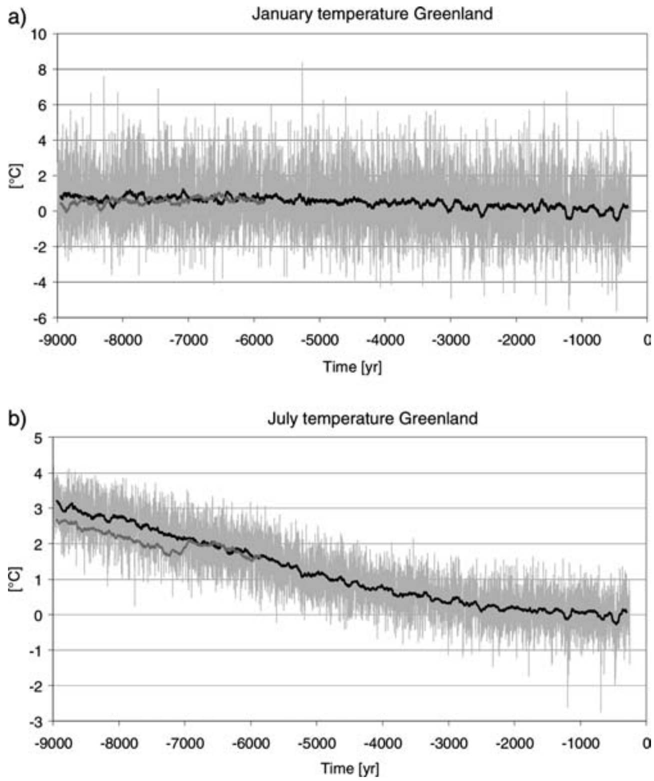

Fig. 7 Simulated surface temperature (°C) evolution for Greenland (62–84°N, 54–31°W), shown as deviations from the preindustrial mean (1,000–250 yr BP). **a**January, **b** July. The unfiltered results of MAIN are shown by the *thin gray line*, whereas the *thick lines* represent the 100-point running averages of MAIN (*black*) and ICE (*dark gray*). The preindustrial means for January and July temperatures are −23.4 and −0.7°C, respectively

relatively strong response during January reflects the impact of the Arctic Ocean, where a maximum temperature difference was noted in winter (see Fig. 4a).

3.2 Precipitation

According to the simulation results, most of our study area experiences a decrease in summer precipitation (Fig. 9), whereas the winter precipitation remains at approximately the same level (Table 1). Indeed, in our experiment, summer is the season with the largest changes in precipitation, so that the pattern of annual mean precipitation change (not shown) is similar to the picture for summer. Scandinavia forms an exception, as the summer precipitation is not changing here (Fig. 10a and Table 1), although locally a decrease is noted on the 0 –9 k-anomaly map (Norwegian coast, Fig. 9). In the other regions, the reductions in summer precipitation over 9 kyr are much more substantial (29, 7 and 17% for North America, Greenland and northern Eurasia, respectively, Fig. 10b–d and Table 1). However, the values for North America and Greenland should be lowered, as the residual Laurentide Ice Sheet in ICE caused the summer precipitation to be reduced by 5–10 mm month^{-1} compared to MAIN. The summer precipitation shows a considerable decrease in interannual variability in all regions, i.e. an opposite trend to what was found for temperature (Table 1).

3.3 Atmospheric circulation

The simulated atmospheric circulation changes considerably throughout the experiment, especially in autumn, which is the season with the largest temperature decrease in the Arctic (see above). In this season, the geopotential height at 850 hPa and surface pressure increase substantially at high latitudes (Fig. 11a), while they decrease at mid-latitudes. As a consequence, the meridional pressure gradient decreases during SON and the mid-latitude westerlies experience a marked weakening (not shown). A reduced zonality of the atmospheric circulation means less effective heat transport from the oceans to downwind continents, thus probably contributing to the decrease in temperatures in northern Europe and Beringia. Those anomalies in the atmospheric circulation project strongly on the Arctic Oscillation (AO)(Thomson and Wallace 1998), defined here as the first EOF of the geopotential height at 850 hPa, and the AO index significantly

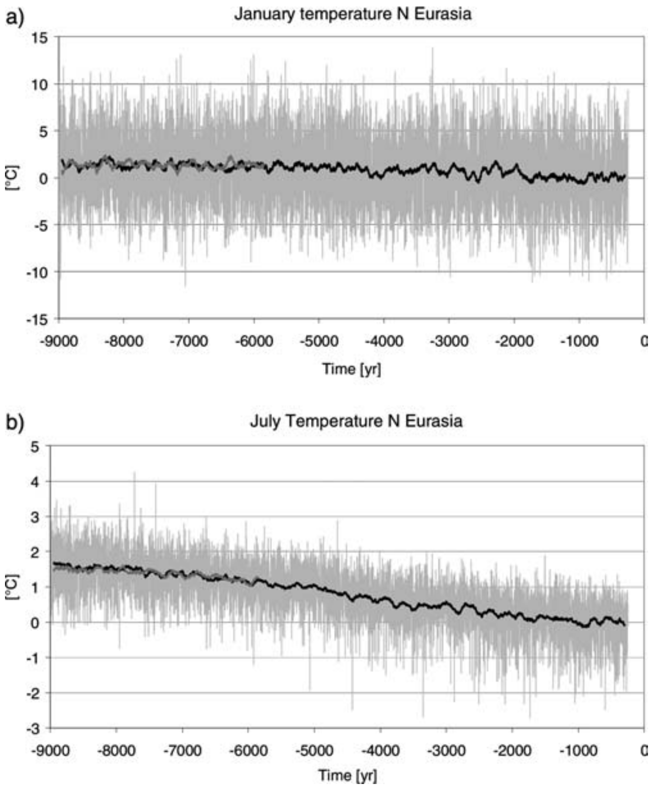

Fig. 8 Simulated surface temperature (°C) evolution for Northern Eurasia (62–78°N, 75–148°E), shown as deviations from the preindustrial mean (1,000–250 yr BP). **a**January, **b** July. The unfiltered results of MAIN are shown by the *thin gray line*, whereas the *thick lines* represent the 100-point running averages of MAIN (*black*) and ICE (*dark gray*). The preindustrial means for January and July temperatures are −42.9 and 16.1°C, respectively

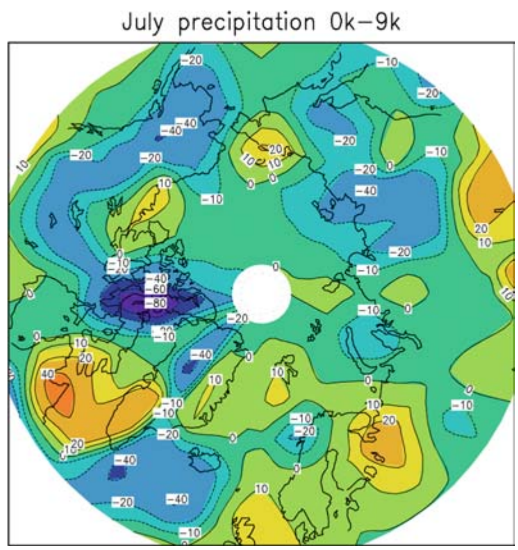

Fig. 9 Simulated July precipitation (mm month^{-1}), preindustrial minus 9–8 k anomaly

decreases in SON during the simulation (Fig. 11b). In DJF, the link between the AO and the long-term trend of the anomalies of atmospheric circulation is less clear, with a weak increase in the AO index in this season.

3.4 Sea ice

As expected, the simulated sea-ice area expands significantly during summer (by 3.5*10^6 km^2, Fig. 12). This expansion is especially expressed during the first 7 kyr of the experiment, thereby following the summer insolation curve (Fig. 1). In the experiment, the sea-ice spreading is especially marked in the Canadian Arctic, the Greenland Sea and in the eastern Barents Sea (Fig. 13a). In Fig. 12, positive anomalies are noted that are simultaneous with the temperature depressions found in the Scandinavian time series around 2.5 and 1.7 kyr BP (Fig. 5). In addition to the larger sea-ice area, a significant increase in the sea-ice thickness is also noted, amounting in the central Arctic Ocean to 2.5 m in September (not shown). Together with the expansion of the ice cover, this leads to an increase in the annual sea-ice volume of 20,000 km^3 (Table 2). The increase in the sea-ice thickness in the central Arctic produces a large increase in the southward sea-ice transport through Fram Strait (Table 2), contributing to the sea-ice expansion east of Greenland. The expansion of the ice cover also results in a substantially higher surface albedo (+30% in core regions, Fig. 13b). In winter, the changes in sea ice are less dramatic, although some expansion is seen south of Svalbard and in the Baffin Bay (Fig. 13c).

3.5 Ocean circulation

The strength of meridional overturning circulation in the Nordic Seas slightly decreases by 0.4 Sv or 12% (Fig. 14 and Table 2), consistent with the noted expansion of winter sea-ice cover here (Fig. 13c). After 4 kyr BP, the temporal variability of this circulation is notably enhanced (Table 2). The overturning in the Nordic Seas is substantially weaker during the two events around 2.5 and 1.7 kyr BP, which are characterized by cooling over northern Europe and an increase in sea-ice cover (Fig. 14). The long-term reduction in overturning circulation in the Nordic Seas is accompanied by a decrease in the convection depth south of Svalbard (Fig. 15). Simultaneously, however, deep convection is enhanced in the Labrador Sea, which is coherent with the small increase in the overall North Atlantic overturning circulation as expressed by a slightly larger NADW export at 20°S (Table 2). The northward heat transport by the North Atlantic Ocean at 20°S remains constant, as it varies around a mean of 0.32×10^{15} W throughout the experiment.

3.6 Vegetation

In our experiment, the length of the growing season becomes shorter as a result of the decreasing summer insolation. This is signified by a decrease in the GDD0 (growing–degree days) index, which expresses the annual sum of the continental air surface temperatures for days

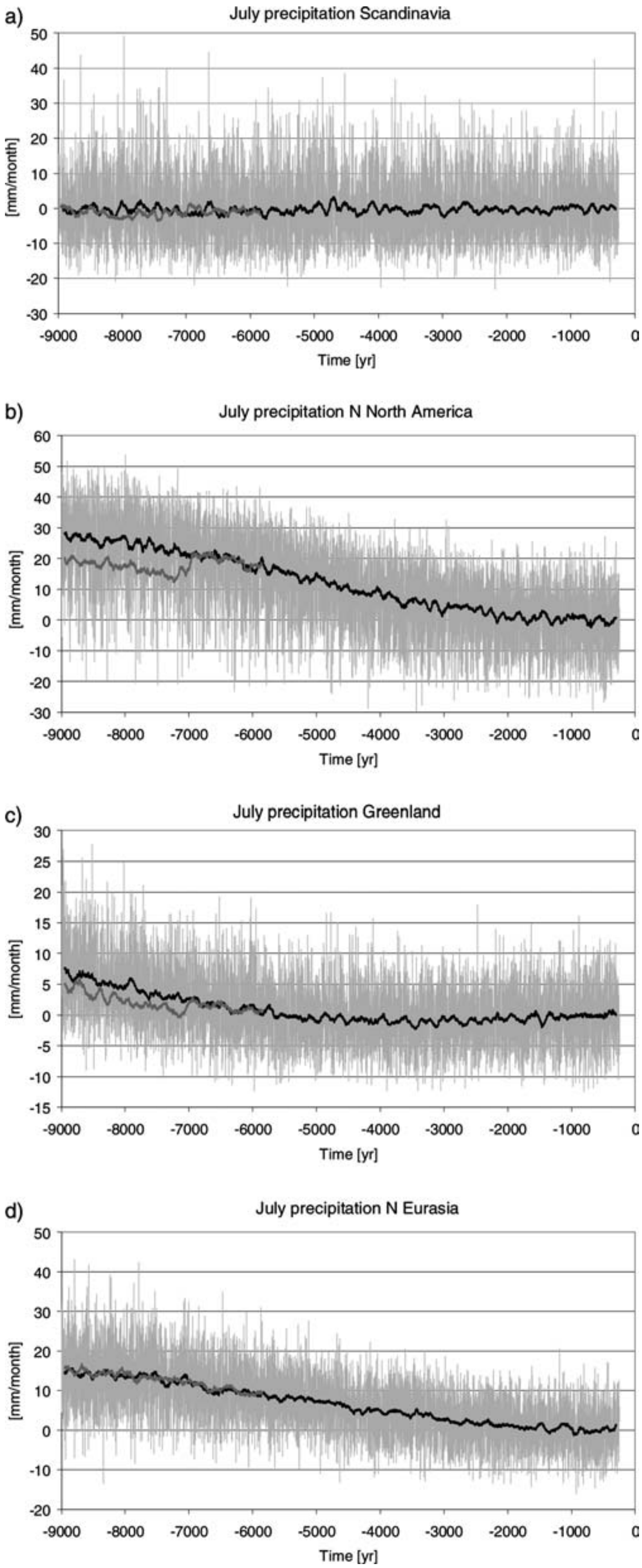

◀

Fig. 10 Simulated July precipitation (mm) evolution, shown as deviations from the preindustrial mean (1,000–250 yr BP). **a** Scandinavia (preindustrial mean = 45.9 mm), **b** northern North America (preindustrial mean = 62.9 mm), **c** Greenland (preindustrial mean = 63.7 mm) and **d** northern Eurasia (preindustrial mean = 65.7 mm). The unfiltered results of MAIN are shown by the *thin gray line*, whereas the *thick lines* represent the 100-point running averages of MAIN (*black*) and ICE (*dark gray*)

with temperatures exceeding 0°C. Averaged over the area north of 60°N, the GDD0 index decreases moderately by 210 from 1,490 to 1,280 degree days (Fig. 16a). Since temperature is one of the main factors controlling vegetation cover at the high northern latitudes, the

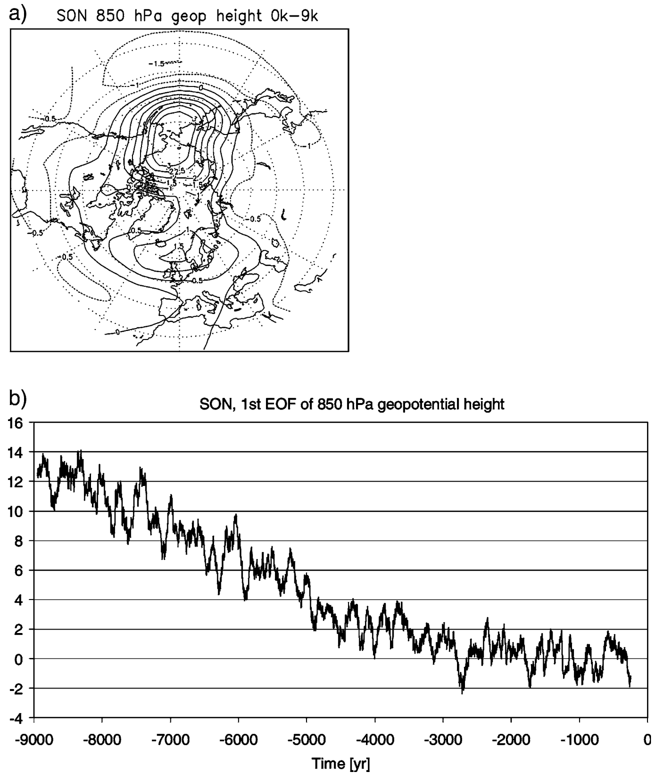

Fig. 11 Simulated changes in atmospheric circulation in SON. **a** Preindustrial minus 9–8 k anomaly map for 850 hPa geopotential heights (in dam) and **b** time series of the first EOF of the 850 geopotential height anomaly (i.e., the simulated Arctic Oscillation index)

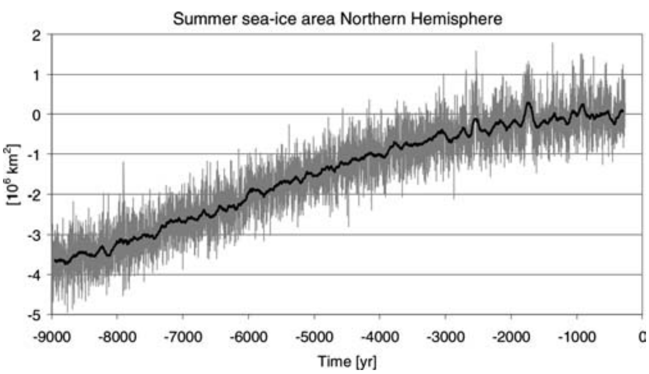

Fig. 12 Simulated summer sea-ice area (10^6 km^2) in the Northern Hemisphere, shown as deviations from the preindustrial mean ($12.2*10^6$ km^2, 1,000–250 yr BP). The 100-point running average (*thick line*) and the unfiltered results (*gray thin line*) are shown

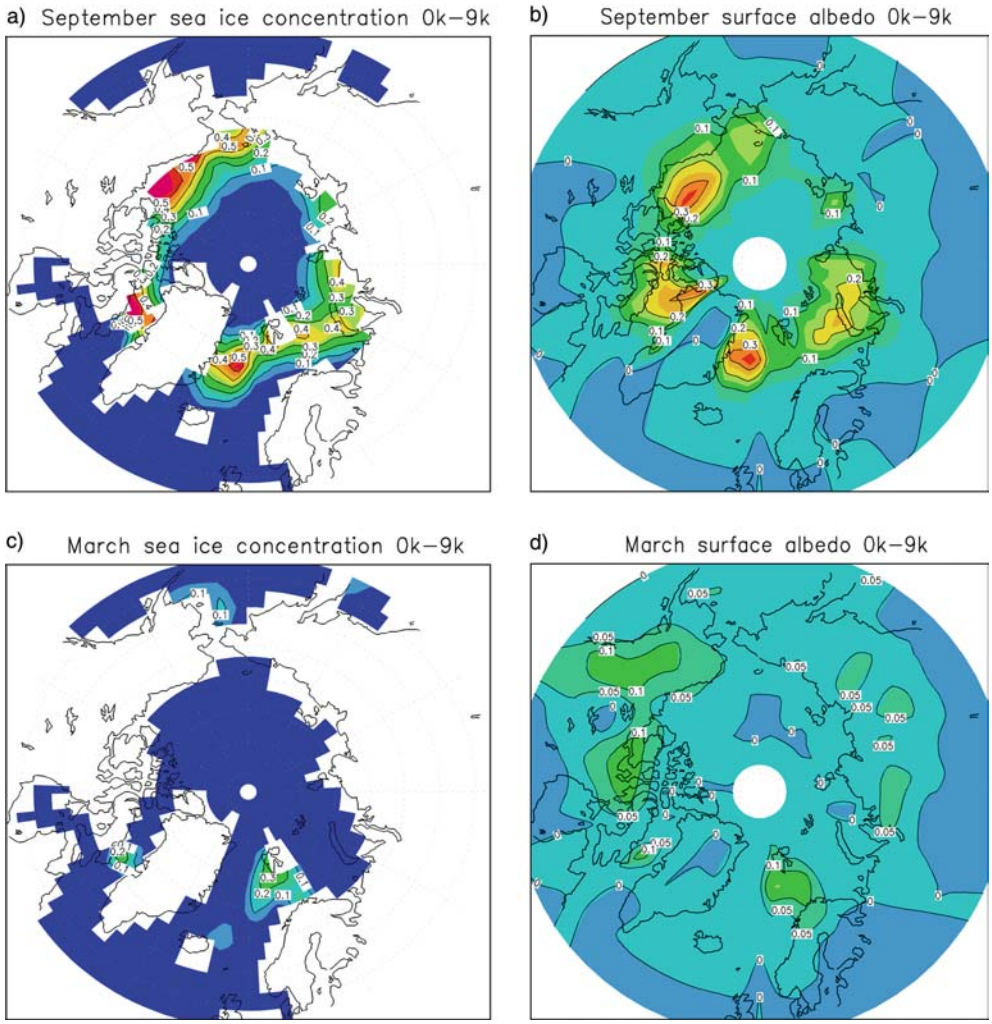

Fig. 13 Preindustrial minus 9–8 k anomaly maps for **a** September sea-ice concentration, **b** September surface albedo, **c** March sea-ice concentration, **d** March surface albedo

Table 2 Some absolute annual mean results from the ocean model for four time periods: Early Holocene (9–7 kyr BP), Mid Holocene (7–4 kyr BP), Late Holocene (4–1 kyr BP) and preindustrial (1000–250 yr BP)

Simulated variable	Time periods (kyr BP)			
	9–7	7–4	4–1	Preindustrial
Max. meridional overturning in Nordic Seas (Sv)	3.26	3.17	2.98	2.92
SD	0.24	0.25	0.34	0.34
NADW export at 20°S (Sv)	13.58	13.74	13.82	13.84
SD	0.84	0.87	0.86	0.88
Sea-ice area in the Northern Hemisphere (10^6 km^2)	11.08	11.56	12.04	12.19
SD	0.28	0.32	0.33	0.32
Sea-ice volume in the Northern Hemisphere (10^3 km^3)	21.43	28.98	39.35	42.83
SD	1.97	3.71	3.57	3.22
Northward water transport between Iceland-Norway (Sv)	11.09	11.14	11.25	11.23
SD	0.72	0.79	0.90	0.90
Southward water transport through Fram Strait (Sv)	3.17	3.07	2.93	2.91
SD	0.43	0.51	0.62	0.66
Southward water transport through Denmark Strait (Sv)	8.27	8.34	8.50	8.51
SD	0.89	0.92	1.08	1.08
Southward sea-ice transport through Fram Strait (Sv)	0.044	0.054	0.066	0.071
SD	0.011	0.015	0.018	0.020

The annual standard deviations (SD) are also shown

shortening of the growing season is responsible for a decrease in the fractional forest cover by 0.09 (from 0.45 to 0.36, Fig. 16b). The maximum decrease in forest fraction is found in North America (up to 0.35 decrease, Fig. 17a, b), where it results in a 12% increase in the surface albedo in September (Fig. 13b). In Scandinavia and northern Eurasia, the reduction in forest fraction (Fig. 17a) is smaller and reaches locally 0.15–0.20,

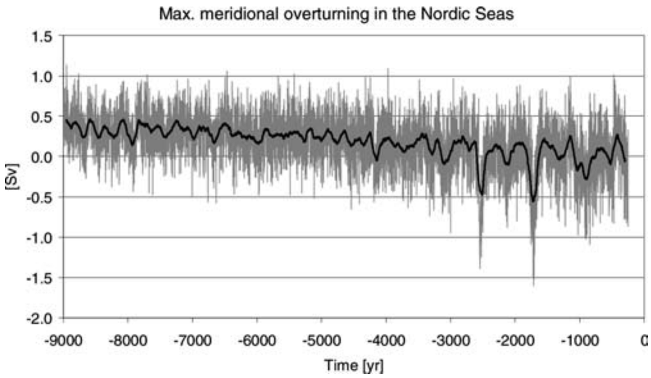

Fig. 14 Evolution of the annual maximum meridional overturning streamfunction (Sv) in the Nordic Seas, shown as deviations from the preindustrial mean (2.9 Sv, 1,000–250 yr BP). The 100-point running average (*thick line*) and the unfiltered results (*gray thin line*) are shown.

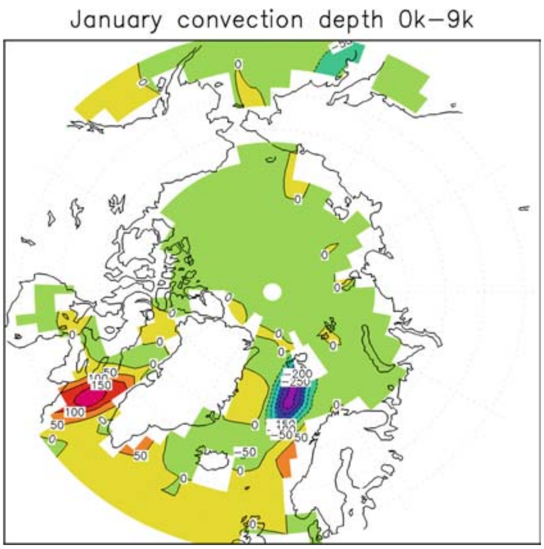

Fig. 15 Simulated preindustrial minus 9–8 k anomaly map for the convection depth (m) in January

leading to a 5% rise of the surface albedo here in September. Most of the reduction (about two-thirds) in forest fraction takes place after 6 ka BP (Fig. 17b).

4 Comparison with proxy data

4.1 Northern Europe

Proxy data from northern Europe suggest that the timing of the thermal optimum varied from region to region. Reconstructions of summer temperatures, based on the altitude of former Pine tree-limits in southern Norway (~60°N) and central Sweden (63°N), suggest an early Holocene optimum between 9–8 kyr BP (Dahl and Nesje 1996). Similarly, a pollen-based reconstruction from the Norwegian coast at 70°N suggests a thermal optimum starting just before 9 kyr BP and lasting until

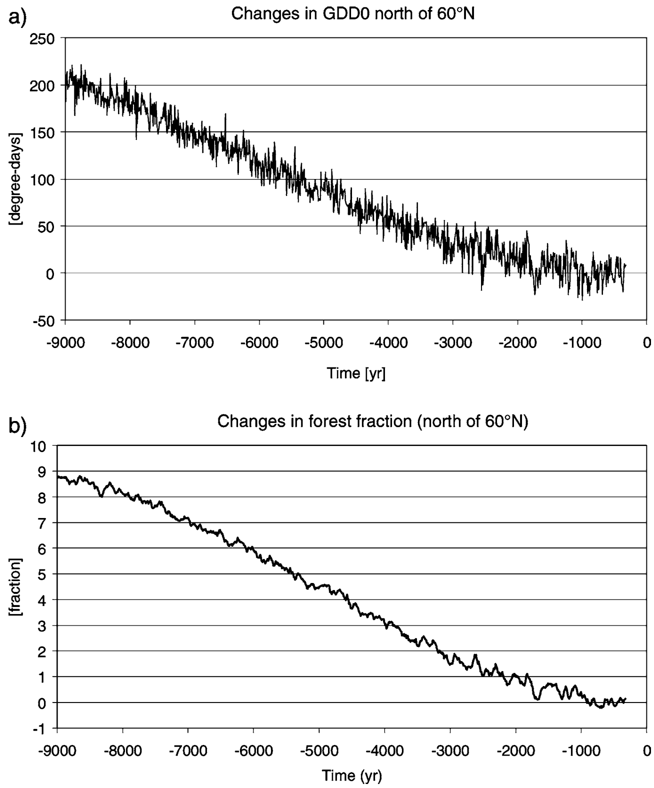

Fig. 16 Simulated time series (10-year means) of **a** changes in GDD0 and **b** changes in fraction of land surface covered by forest, shown as deviations from the preindustrial mean (1,000–250 yr BP). Both are calculated for the area north of 60°N. The preindustrial means for GDD0 and forest fraction are 1,287 degree days and 0.37, respectively

6.5 kyr BP (Seppä et al. 2002), consistent with SST reconstructions in the Nordic Seas (e.g., Birks and Koç 2002). More inland, however, summer temperature reconstructions from northern Finland (~69°N) based on diatoms (Korhola et al. 2000) and pollen (Seppä and Birks 2001, 2002) indicate that the optimum was somewhat later and peaked between 8 and 6 kyr BP. The estimated amount of summer cooling during the Holocene is consistent throughout the region and amounts to 1–1.5°C. Our model results are in good agreement with this range of summer cooling, as the July temperatures are 1.2°C warmer in the early part of the experiment (9–7 kyr BP) compared to the last 0.5 kyr (Table 1).

The simulated timing of the thermal maximum between 9 and 8 kyr BP (Fig. 5b) is consistent with most sites, although we find no sign of a delayed thermal optimum as reported for Northern Finland, but this lag is probably caused by local effects (e.g., vegetation development, topography) not resolved by our model. Reconstructions of precipitation in northern Europe suggest that the early Holocene (9–7 kyr BP) was relatively humid compared to the present day (Seppä and Hammarlund 2000; Hammarlund et al. 2002). The estimates of the reduction in precipitation during the Holocene vary between −30%, on an annual basis based on pollen (Seppä and Birks 2001), and −40 to −50% for

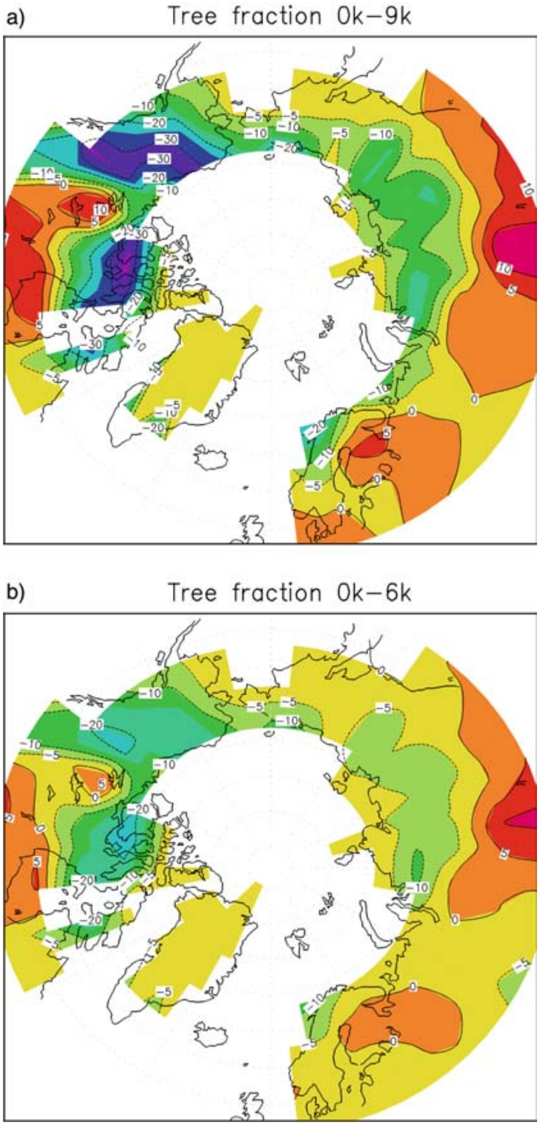

Fig. 17 Simulated anomalies of the forest fraction, **a** preindustrial minus 9–8 k and **b** preindustrial minus 6–5 k

winter based on equilibrium line altitudes of glaciers (Dahl and Nesje 1996; Nesje et al. 2001). The model experiment has not captured this marked decrease in precipitation (Fig. 10a), although a reduction is simulated in Northern Scandinavia (Fig. 9). Moreover, the simulated decrease in zonal circulation during SON agrees with the reconstructions for northern Sweden (Hammarlund et al. 2002).

Many proxy records from northern Europe show evidence for millennial-scale fluctuations that are superimposed on the long-term cooling trend (Dahl and Nesje 1996; Korhola et al. 2000; Nesje et al. 2001; Seppä and Birks 2001). These millennial-scale events are not reproduced in our experiment. This is not surprising, as we did not prescribe any changes in the forcing at this time-scale. In particular, the cooling events have been associated with variations in solar irradiance, possibly causing temporary weakening of the thermohaline circulation (THC; Bond et al. 2001; Goosse et al. 2002b). A special case is the pronounced cooling event around 8.2 kyr BP, when a THC weakening was probably triggered by a meltwater pulse associated with the final deglaciation of the Laurentide Ice Sheet (Alley et al. 1997; Barber et al. 1999; Renssen et al. 2001). Besides, the model simulates large cold events at decadal to centennial timescales (Fig. 5). The proxy records in Scandinavia do not have a sufficient temporal resolution to have registered such a type of event. A possible exception is a speleothem from northern Norway, which produced a high-resolution temperature record that shows a few prominent negative excursions (~2°C magnitude) at a decadal–centennial scale (Lauritzen and Lundberg 1999) during the last 4 kyr BP. The simulated July temperature anomalies (Fig. 5b) show a reasonable correspondence with the latter excursions, suggesting that the progressive increase in the variability of the THC strength could have taken place in the real world during the Holocene.

4.2 Northern North America

For northern North America, there is considerable evidence for a thermal optimum in the early Holocene in northwest Canada and Beringia (9–8 kyr BP, in Alaska even starting earlier; see e.g., Ritchie et al. 1983; Bradley 1990; Kaufman et al. 2004). An example of an early optimum is provided by the melt record from the Agassiz Ice cap, indicating that the warmest summers occurred between 9–8 kyr BP (Koerner and Fisher 1990). A warm early Holocene is also suggested by the findings of bones and tusks of marine mammals (Walrus, Bowhead and Narwhal) and of thermophylous molluscs, far beyond their present normal range, and dated to 9–7 kyr BP, indicating reduced sea-ice conditions compared to the present day in the Canadian Arctic (Harington 1975; Stewart and England 1983; Bradley 1990; Dyke and Savelle 2001). In addition, fossils of Caribou found at 82°N (northernmost Ellesmere Island), dated before 9 kyr BP, show that summer conditions on land must have been mild in the early Holocene (Steward and England 1986). Furthermore, certain plant species were much more distributed northward than at present (Ovenden 1988), and some glaciers had smaller extensions than today (Bradley 1990). Reconstructions of sea surface conditions in the northern Baffin Bay suggest open waters as early as 8.5 kyr BP, with temperatures up to 3°C warmer than today (Levac et al. 2001). There is some evidence (from peat growth in NW Canada) that this early optimum was more humid than later in the Holocene (Vardy et al. 1998). Paleoecological data suggest that at 6 kyr BP, the tree line was located 100 km north of its modern position in the MacKenzie delta, but no change in forests was found in Western Alaska (Bigelow et al. 2003).

Proxy evidence from eastern Canada (most notably Quebec and Labrador) indicates that the thermal maximum started a few thousand years later (between 8–6 kyr BP, e.g., MacDonald et al. 1993; Kaufman et al. 2004). This delay has been attributed to the chilling effect of the residual Laurentide Ice Sheet (Kaufman et al. 2004). The latter moderation of the thermal conditions was probably also responsible for the more southward position of the 6 kyr BP tree line in eastern Canada compared to the present day (Bigelow et al. 2003), i.e. the opposite effect to what is found in the MacKenzie delta.

Mild conditions appear to have persisted until 5 to 4 kyr BP (Steward and England 1983; Bradley 1990; Dyke and Savelle 2000; Kaufman et al. 2004). After 4 kyr BP, enhanced cooling is registered in many records. Glaciers experienced widespread expansion (Bradley 1990) and the sea-ice cover in the area became much more extensive (Stewart and England 1983), with the Baffin Bay becoming perennially ice-covered again (Levac et al. 2001). In addition, pollen and peat records in arctic Canada also have registered widespread cooling after 4 kyr BP (Williams and Bradley 1985; Vardy et al. 1998; Gajewski and Frappier 2001). Finally, the melt-record from the Agassiz ice core suggests that the coldest summers (very low melt) occurred in the last 2.5 kyears (Koerner and Fisher 1990).

The model results generally show a good agreement with this proxy evidence for northern North America. The early optimum noted for northwestern Canada and the enhanced cooling after 5 kyr BP are both present in the simulation (not shown). The delay of the thermal maximum in eastern Canada as a response to the residual Laurentide Ice Sheet is consistent with our idealized ICE experiment. Moreover, in the early part of the experiment (9–7 kyr BP), precipitation in most places is significantly higher than in the preindustrial climate (Fig. 9), which is in agreement with evidence for enhanced peat growth in the early Holocene. However, compared to the 100 km southward tree line shift found in proxy records in the MacKenzie delta, the model appears to have overestimated the response of the vegetation, as seen in the strong reduction in forest fraction in Fig. 16a, b.

4.3 Greenland

The ice-core records from central Greenland suggest that Holocene cooling was more pronounced at northern sites than in the south. The NorthGRIP record (75°N) shows a more prominent thermal optimum (δ^{18}O values 0.6‰ higher) between 8.6 and 4.3 kyr BP than the GRIP core (72°N) (Johnsen et al. 2001). The estimated summer cooling that followed this optimum is 3°C for NorthGRIP. This picture is confirmed by lake records from southern Greenland, showing a thermal optimum between 8 and 5 kyr BP and an expressed cooling after 3 kyr BP (Kaplan et al. 2002). Our model results (Fig. 7) show a very similar amount of cooling (3°C) during summer as in NorthGRIP. In addition, the simulated cooling is stronger in northern Greenland than in the south (Fig. 4c), which is in agreement with the difference between NorthGRIP and GRIP. However, the clear climatic optimum is lacking in the main simulation, which may be caused by the lack of a residual Laurentide Ice Sheet in this experiment, as our ICE simulation produced a flatter summer temperature evolution over Greenland between 9 and 6 kyr BP (Fig. 7b). Our simulation also displays a clear change in the seasonality of precipitation during the Holocene, as the ratio between summer and winter precipitation decreases by about 10%. As the isotope composition of the snow is influenced by the season at which snow accumulates, such a change in the seasonality of precipitation could bias our interpretation of isotope-based reconstructions (e.g., Werner et al. 2000).

4.4 Northern Eurasia

Numerous studies indicate that from 9 to 4 kyr BP, the tree line in northern Eurasia was situated a few hundred kilometers more northward than today (e.g., TEMPO members 1996; MacDonald et al. 2000; Prentice et al. 2000 Andreev et al. 2001; Naidina and Bauch 2001; Bigelow et al. 2003), indicative of warmer summers in the early and mid Holocene. For instance, Andreev and Klimanov (2000) estimate for the Taymyr peninsula a gradual summer cooling of 2–1°C from the early Holocene to the present, accompanied by a decrease in annual precipitation of 50 mm year^{-1}. Here and at other sites, this gradual trend is interrupted by several millennial-scale events, possibly equivalent to those found in the Atlantic region. For the same region, Brovkin et al. (2002) simulate decreases in reconstructed forest fraction during the Holocene, especially after 4 kyr BP. Our model produced a long-term cooling of ~1.5°C (Figs. 4c, 8b) and a precipitation reduction (Fig. 10d) that agrees well with this paleoclimatic evidence. The model appears to somewhat underestimate the southward retreat of the tree line seen in the data, as the simulated reduction in forest fraction (Fig. 17) does not exceed 0.15 in northern Eurasia (i.e. from 0.35–0.55 at 9 kyr BP to 0.20–0.40 at 0 kyr BP).

4.5 Nordic Seas

Oceanic proxy data indicate that in the Nordic Seas the Holocene climate evolution was different for the eastern and western part. Based on diatom analyses, Koç et al. (1993) concluded that around 10 kyr BP, conditions in the eastern Nordic Seas were already comparable to the present day, with an inflow of warm Atlantic waters, whereas in the western Nordic Seas the surface was still cooler with a relatively extensive sea-ice cover. The thermal optimum was reached in the entire Nordic Seas around 9 kyr BP, with substantially warmer conditions than at present (e.g., Andersen et al. 2004). During this optimum, warm Atlantic waters dominated the eastern part of the basin, while arctic conditions were present only in a narrow zone along the Greenland coast (Koç et al. 1993). This picture is confirmed by studies based on foraminifera. For instance, Bauch et al. (1999) found that in the central Nordic Seas, the lowest concentrations of the polar species *Neogloboquadrina pachyderma* (left coiling) were found between 9 and 6 kyr BP. Similarly, Rasmussen et al. (2002) concluded based on foraminifera that a strong inflow of warm Atlantic waters in the Faroe-Shetland region started around 9.5 kyr BP and the rate of mass exchange reached a maximum at 6.5 kyr BP (stronger inflow and stronger outflow). Following the optimum, the polar and arctic fronts moved gradually in a southeasterly direction, leading to an expansion of the sea-ice cover, particularly in the Greenland Basin after ~5 kyr BP (Koç et al. 1993; Koç and Jansen 1994). This expansion is accompanied by an increase in variability, especially in the last millennium (Andersen et al. 2004). Reconstructions of sea surface temperatures indicate that the total Holocene summer cooling was in the order of 2–3°C (Salvigsen et al. 1992; Koç et al. 1996; Marchal et al. 2002), although the cooling may have been more substantial (5°C) in the northern Nordic Seas (Koç et al. 1996). According to Koç et al. (1993), the evolution of winter sea surface temperatures closely followed the summer trend.

In our experiment, the overall Holocene summer cooling in the Nordic Seas is of the same order (1–2°C, Fig. 4c) as suggested by the proxy data. In addition, the model seems to have captured the sea-ice expansion in the western part of the Nordic Seas reasonably well (Fig. 13), including the increase in variability. However, the simulated change in overturning circulation shows no sign of the mid-Holocene maximum found by Rasmussen et al. (2002). In our experiment, the meridional overturning circulation in the Nordic Seas weakens from 9 to 0 kyr BP, resulting in enhanced cooling (5°C annual mean) near Svalbard, i.e. the main site of deep convection. The simulated reduction in meridional overturning is consistent with proxy evidence from the northeastern North Atlantic, suggesting reduced NADW formation in the Nordic Seas after 7–6 kyr BP (Solignac et al. 2004).

4.6 Barents Sea

In the Barents Sea, the start of the Holocene was similar as in the Nordic Seas, as proxy data indicate that the inflow of warm Atlantic waters started around 10 kyr BP (Duplessy et al. 2001; Voronina et al. 2001). Analyses on foraminifera in a core from the northeastern part (near Franz Josef Land) show a marked optimum from 7.8 to 6.8 kyr BP, with a maximum inflow of Atlantic waters (Duplessy et al. 2001). The optimum was followed by a 1–2°C long-term surface cooling, interrupted by several events at a centennial–millennial scale. In the southeastern part of the basin, dinoflagellate cyst analyses on several cores indicate relatively warm conditions from 8 to 5 kyr BP, followed by colder conditions and expansion of sea ice (Voronina et al. 2001). Reconstructions of the sea-ice cover reveal the occurrence of distinct positive excursions during the last 5 kyr. This picture is confirmed by the glacier records of Franz Josef Land and Svalbard, showing a very similar evolution with widespread glacier advances starting at ~5 kyr BP, followed by fluctuations during the late Holocene (e.g., Lubinski et al. 1999). The simulated climatic evolution of the Barents Sea region gives a reasonable match with the proxy data, showing a long-term cooling trend of 1°C during summer (Fig. 4) and a marked expansion of sea ice (Fig. 13).

5 Discussion and concluding remarks

5.1 Effect of external forcings

Compared to earlier model studies, our results give a similar response to the prescribed external forcings. The simulated long-term summer cooling over the continents north of 60°N follows the prescribed orbital forcing (Fig. 2a). Indeed, the summer temperature depression found over most land surfaces (−1 to −3°C) is similar to what is obtained in equilibrium experiments performed with atmospheric GCMs coupled to mixed layer ocean models to study the impact of orbital forcing at 9 kyr BP (Kutzbach and Gallimore 1988; Mitchell et al. 1988). The general decrease in summer precipitation is a direct consequence of this overall cooling and the range found in our experiment is comparable to that reported by Brovkin et al. (2002). To quantify the contribution of the variations in greenhouse gas concentrations, we performed an additional sensitivity experiment with ECBilt-CLIO-VECODE in which we prescribed only the long-term changes in atmospheric $CH_4$and CO_2 content as shown in Fig. 2. The effect of these greenhouse gas changes in the areas north of 60°N was an almost linear warming trend of 0.5°C over 9 kyr, which is consistent with the findings of Crucifix et al. (2002). This suggests that the greenhouse gas forcing partly counteracts the decrease in summer insolation.

5.2 Impact of internal feedbacks

In addition, we find in our results the impact of several internal feedbacks described in other model studies. First, the well-known snow/ice-albedo positive feedback, involving an increase in the cover of snow and sea ice as a response to decreasing temperatures leading to a higher surface albedo and thus to further cooling (Kerwin et al. 1999; Crucifix et al. 2002). The type of vegetation also influences the albedo of the snow cover, as it is much higher for grasslands than for forests (e.g., Harvey 1988). Second, the sea ice-insulation feedback is important, with a decreasing heat flux from the ocean to the atmosphere when the insulating sea-ice cover becomes thicker. In our experiment, these two feedbacks caused an amplification of the orbitally forced cooling, especially in the Canadian Arctic, as can be deduced from a comparison of the increase in surface albedo (up to +30%, Fig. 13b) and the pattern of the 9–0 kyr BP temperature anomalies (locally −7°C, Fig. 4d). The decrease in summer temperature also leads to a weaker summer melt, and a thicker ice cover in summer as well as in winter. Furthermore, the thermal inertia of the ocean also plays an important role, as it causes a dampening of the orbitally induced summer temperature variations and lead to a lagged response over the oceans, relative to the seasonal cycle of insolation and the more direct response over land surfaces. Considering that the duration of this lag is a few months, both effects caused a clear maximum temperature difference over the Arctic Ocean in the winter half year instead of summer (Fig. 4). This also explains the long-term cooling trend in winter temperatures (Fig. 3a), which shows no sign of a direct response to the increase in insolation (+12 W/m^2) in contrast to the mid-latitudes where a winter increase in temperature is noticed over the continents.

The profound changes in sea ice also affected the Holocene evolution of precipitation in different regions. Measurements in the present-day Canadian Arctic show that the precipitation amounts depend strongly on the sea-ice extent in adjacent basins (e.g., Williams and Bradley 1985). A comparison of the maps showing precipitation anomalies (Fig. 8) and sea-ice changes (Fig. 10), shows that the maximum precipitation reduction (40–60 mm $month^{-1}$) is found in Northern Canada close to the region with maximum expansion in sea-ice cover (up to +60%) during summer and autumn. It is likely that here the ocean surfaces were important as a moisture source during the early part of the experiment. Europe receives its moisture from the Northern Atlantic and the eastern Nordic Seas, both of which remained ice-free throughout the experiment, possibly explaining why the reduction in precipitation is not as striking here (Table 1).

A third important feedback involves the biogeophysical relation between forest fraction and albedo. When the forest cover decreases as a result of the orbitally induced shortening of the growing season, this also amplifies the cooling, as forests have a much lower surface albedo than tree-less vegetation (e.g., Harvey 1988; Foley et al. 1994; TEMPO members 1996; Ganopolski et al. 1998; Brovkin et al. 2002). As analyzed by Brovkin et al. (2003), the strength of this feedback is related to the non-linear dependence of the forest fraction on the GDD0 index. When the summer temperatures decrease and the GDD0 index reaches a certain threshold (which is model dependent), the forest fraction is rapidly reduced, making the biogeophysical feedback stronger. Sensitivity analyses with another coupled model that includes VECODE (i.e. MoBiDiC) have shown that in this case this threshold is about 1,200 degree days (Brovkin et al. 2003). In ECBilt-CLIO-VECODE, the threshold probably has a similar value. In our simulation, the GDD0 index crosses the 1,200 degree-days threshold in some regions in North America (central North Canada and Alaska), i.e. the areas where we found a 0.35 reduction in forest fraction (Fig. 17a) and a 12% rise in surface albedo in spring (Fig. 13d). A substantial part of the temperature reduction in these areas is probably due to this biogeophysical feedback, especially in spring (compare Fig. 4b, c with Fig. 13d). This feedback is amplified via sea ice-related feedbacks discussed above. In transient Holocene simulations performed with MoBiDiC, this vegetation-related amplification of the orbitally forced cooling was found to be responsible for a 1.5°C reduction in summer temperature in the last 4 kyr (Crucifix et al. 2002). There is also a second, less important feedback active at high latitudes in which vegetation plays a role, involving the reduction in evaporation with decreasing forest fraction, leading to increasing summer temperatures (i.e. a negative feedback, e.g., Bonan et al. 1995; Brovkin et al. 2003). However, the latter feedback is not taken into account in our model, as vegetation changes only affect the surface albedo. Consequently, the absence of this negative feedback potentially caused an overestimation of the long-term summer cooling.

5.3 Original features compared to previous Holocene model studies

Compared to previous climate model studies, we have identified a number of novel aspects of Holocene climate change that are consistent with available proxy data. First, our simulation shows a shallower deep convection (by more than 250 m, Fig. 15) and weakened overturning strength (by 0.5 Sv, Fig. 14) in the Nordic Seas, while it is enhanced in the Labrador Sea. The enhancement of the deep convection in the Labrador Sea (by 150 m) is related to the cooling of the surface ocean (up to 6°C in winter), leading to an increase in the surface density (e.g., Rahmstorf et al. 1996). Surface cooling also occurs in the Nordic Seas, but here its effect is overwhelmed by the impact of a marked sea-ice expansion in the region of deep convection, accompanied by a slight decrease in surface salinity (−0.25 psu over 9 kyr), which stabilizes the upper ocean and reduces deep mixing. In contrast to the Nordic Seas, the main sea-ice expansion in the Labrador Sea is located to the north of the main convection site (Fig. 13) and the surface salinity remains at the same level. The opposite evolution of convection depth in the two regions reflects on the temperature, which shows a stronger decrease in the Nordic Seas compared to the Labrador Sea. This model result is in excellent agreement with paleoceanographical evidence, suggesting that deep-water formation in the Labrador Sea increased during the Holocene, whereas the contribution of Nordic Sea components of the North Atlantic Deep Water decreased (Hillaire-Marcel et al. 2001; Solignac et al. 2004). In the model, the net effect of the opposite changes in the two regions is a small, statistically insignificant increase in the export of NADW out of the Atlantic (Table 1).

A second novel result of our experiment is the increase in variability of the coupled system towards the Late Holocene. This is clearly evident in the temperatures in Scandinavia and North America (Figs. 5, 6 and Table 1), in the different components of the ocean circulation in the Nordic Seas (Fig. 14and Table 2) and in the sea-ice evolution (Table 2). The enhanced variability is most clearly expressed in the Nordic Seas region, where it culminates in two decadal-scale events that are characterized by cooling in Northern Europe (−15°C in January temperature, Fig. 5), negative excursions in overturning strength (−1.5 Sv, Fig. 14) and positive anomalies in the sea-ice extent (Fig. 12). As discussed in detail by Goosse et al. (2003), sea-ice anomalies in the Nordic Seas are part of the internal variability of our model, i.e. they occur in experiments without time-varying forcing. The events are triggered by specific atmospheric conditions, with a negative geopotential height anomaly over Greenland and a positive anomaly over the Nordic and Barents Seas. This atmospheric circulation pattern causes an increase of sea-ice transport towards the Svalbard area, which weakens (or even locally shuts down) the deep convection that is present here in normal years. As a result, the sea-ice area expands even further, enforcing the specific atmospheric circulation pattern and causing strong regional cooling. However, this enhanced cooling also makes the surface ocean waters denser, thus producing a strengthening of the overturning circulation, ending the cold events after a decade or so. Earlier sensitivity experiments have shown that the frequency of sea-ice anomalies increases substantially when the climate becomes colder, as this enhances the probability of inference of sea ice and deep convection in the Nordic Seas (Goosse et al. 2003; Goosse and Renssen 2004). The simulated increase in variability towards the Late Holocene is thus related to the interaction between sea-ice expansion and deep convection. Our result is consistent with high-resolution proxy data from the Nordic Seas that indeed suggest expansion of the sea-ice cover and an increase in the variability, especially in the western part of the basin during the last 1 kyr (Andersen et al. 2004). Moreover, detailed marine and terrestrial records indicate the occurrence of several striking decadal-scale cooling events during the last 3 kyr (Lauritzen and Lundberg 1999; Andersson et al. 2003) that may reflect similar conditions as the two events in our experiment.

A third original outcome of our simulation is the decrease in the zonality of the atmospheric circulation during the Holocene, as reflected by a decline in the meridional pressure gradient and a reduction of the AO index, especially during autumn in the first 5 kyr. Again, this result is consistent with proxy data giving information on the atmospheric circulation (Hammarlund et al. 2002; Andersen et al. 2004). A similar effect on the atmospheric circulation was found by Tuenter et al. (2004), who performed sensitivity experiments with ECBilt-CLIO to study the effect of precession on climate. They found that the insolation during minimum precession (e.g., early Holocene) causes winter conditions to start earlier in the North Atlantic region, relative to a situation with maximum precession. Just as in the early part of our experiment, the earlier winter conditions associated with minimum precession result in a higher AO-index in autumn.

5.4 Summary model-data comparison and future perspectives

Generally, our model results are consistent with the proxy evidence discussed, as seen in the model-data agreement for the long-term evolution in temperature, precipitation, sea ice, oceanic circulation and atmospheric circulation. This suggests that most of the long-term trends at high northern latitudes can be explained by the response of the coupled system to orbital and greenhouse gas forcing. Compared to earlier Holocene climate simulation studies (e.g., Weber 2001; Brovkin et al. 2003; Crucifix et al. 2002), we have used a more comprehensive model, which enabled us to explain several new aspects of Holocene evolution found in proxy records. For instance, the use of a 3-dimensional ocean model enabled us to simulate the contrast in deep convection activity between the Nordic Seas and the Labrador Seas, and to show that this is related to competing effects of surface cooling and sea-ice expansion. Also, the application of a comprehensive sea-ice model permits us to show that sea-ice advection is an important process for the Holocene climate evolution. The simulated increase in variability depends partly on southward sea-ice transport through Fram Strait, which in our experiment shows an increase in both the volume flux as in the variability (Table 2). In addition, the use of an atmospheric model resolving synoptic variability allowed us to reproduce the decrease in AO index found in proxy data and to link it to precession. Finally, the incorporation of a dynamic vegetation model revealed the regional importance of biogeophysical feedbacks.

However, some discrepancies between our model result and data that are linked to the limitations of our model were also found. The most important one is the timing of the thermal maximum. Although in many regions the simulated early (9–8 kyr BP) optimum fits the data (Alaska, western Canada, Nordic Sea region), there are also regions where proxy evidence suggests it starts 1–2 kyr later and also lasts longer; for instance eastern Canada, Greenland and inland Scandinavia. The mismatch in eastern Canada and Greenland is related to the lacking of a dynamic ice-sheet model in our simulation. Ideally, one would start a transient Holocene simulation within the Younger Dryas (e.g., at 11 kyr BP), so that the deglaciation is accounted for. This type of simulation will be feasible in the near future, as deglaciation scenarios are available (e.g., Licciardi et al. 1998; Peltier 1994) and the development of dynamic ice-sheet models that can be coupled to climate models is progressing (e.g., Calov et al. 2002). As our model is not yet capable of simulating such a deglaciation scenario, we have attempted to capture the first-order effect of the residual Laurentide Ice sheet on climate by performing our ICE experiment. Although highly idealized, the ICE experiment shows that the effect of the Laurentide Ice sheet would be to delay and flatten the thermal optimum in eastern Canada and Greenland, which is in better agreement with proxy evidence. A second future improvement would be to simulate the Holocene with a higher spatial resolution than the 5.6×5.6° latitude–longitude of our model. This would improve the model-data comparison, as proxy data often represent a more local spatial scale than resolved by this model resolution, due to, e.g., the effect of topography (Renssen et al. 2004). Third, we have used a model with a correction in the freshwater fluxes, which was applied to obtain a correct modern climate state (as explained in Sect. 2.1). It would clearly be preferable to run a model without such flux corrections, as these could influence several aspects of the model, for instance the THC response. Nevertheless, earlier paleoclimate simulations with ECBilt-CLIO have produced results with a good correspondence with paleodata (e.g., Renssen et al. 2002), giving some confidence in the capability of the model to reproduce climate variations under different forcing conditions.

Acknowledgements The useful comments of the two anonymous reviewers are gratefully acknowledged. HR is supported by the Netherlands Organization for Scientific Research. TF and HG are Research Associates at the Belgian National Fund for Scientific Research. This study was carried out as part of the Belgian Second Multiannual Scientific Support Plan for a Sustainable Development Policy (Belgian Federal Science Policy Office, contract EV/10/9A) and the European Research Program on Environment and Sustainable Development (European Commission, contract EVK2-2001-00263). J.M. Campin (MIT) is thanked for programming the coupling of VECODE to ECBilt and for model testing.

References

Alley RB, Mayewski PA, Sowers T, Stuiver M, Taylor KC, Clark PU (1997) Holocene climatic instability—a prominent, widespread event 8200 yr ago. Geology 25:483–486

Andersen C, Koç N, Jennings J, Andrews JT (2004) Nonuniform response of the major surface currents in the Nordic Seas to insolation forcing: implications for the Holocene climate variability. Paleoceanography 19:PA2003. DOI: 10.1029/2002PA000873

Andersson C, Risebrobakken B, Jansen E, Dahl SO (2003) Late Holocene surface ocean conditions of the Norwegian Sea (Vøring Plateau). Paleoceanography 18:1044. DOI: 10.1029/2001PA000654

Andreev AA, Klimanov VA (2000) Quantitative Holocene climatic reconstruction from Arctic Russia. J Paleolimnol 24:81–91

Andreev AA, Manley WF, Ingolfsson O, Forman SL (2001) Environmental changes on Yugorski Peninsula, Kara Sea, Russia, during the last 12,8000 radiocarbon years. Global Planet Change 31:255–264

Barber DC, Dyke A, Hillaire-Marcel C, Jennings AE, Andrews JT, Kerwin MW, Bilodeau G, McNeely R, Southon J, Morehead MD, Gagnon J-M (1999) Forcing of the cold event of 8,200 years ago by catastrophic drainage of Laurentide lakes. Nature 400:344–348

Bauch HA, Erlenkeuser H, Fahl K, Spielhagen RF, Weinelt MS, Andruleit H, Henrich R (1999) Evidence for a steeper Eemian than Holocene sea surface temperature gradient between Arctic and sub-Arctic regions. Palaeogeogr Palaeoclim Palaeoecol 145:95–117

Berger AL (1978) Long-term variations of daily insolation and Quaternary climatic changes. J Atmos Sci 35:2363–2367

Bigelow NH, Brubaker LB, Edwards ME, Harrison SP, Prentice IC, Anderson PM, Andreev AA, Bartlein PJ, Christensen TR, Cramer W, Kaplan JO, Lozhkin AV, Matveyeva NV, Murray DF, McGuire AD, Razzhivin VY, Ritchie JC, Smith B, Walker DA, Gajewski K, Wolf V, Holmqvist BH, Igarashi Y, Kremenetskii K, Paus A, Pisaric MFJ, Volkova VS (2003) Climate change and Arctic ecosystems: 1 Vegetation changes north of 55°N between the last glacial maximum, mid-Holocene, and present. J Geophys Res 108:8170. DOI: 10.1029/2002JD002558

Birks CJA, Koç N (2002) A high-resolution diatom record of late-Quaternary sea-surface temperatures and oceanographic conditions from the eastern Norwegian Sea. Boreas 31:323–344

Bonan GB, Chapin FS III, Thompson SL (1995) Boreal forest and tundra ecosystems as components of the climate system. Clim Change 29:145–167

Bond GC, Kromer B, Beer J, Muscheler R, Evans MN, Showers W, Hoffmann S, Lotti-Bond R, Hajdas I, Bonani G (2001) Persistent solar influence on North Atlantic climate during the Holocene. Science 294:2130–2133

Braconnot P, Marti O, Joussaume S, Leclainche Y (2000) Ocean feedback in response to 6 kyr BP insolation. J Clim 13:1537–1553

Bradley RS (1990) Holocene paleoclimatology of the Queen Elizabeth Islands, Canadian High Arctic. Quat Sci Rev 9:364–384

Brovkin V, Bendtsen J, Claussen M, Ganopolski A, Kubatzki C, Petoukhov V, Andreev A (2002) Carbon cycle, vegetation and climate dynamics in the Holocene: experiments with the CLIMBER-2 model. Global Biogeochem Cycle 16. DOI: 10.1029/2001GB001662

Brovkin V, Levis S, Loutre MF, Crucifix M, Claussen M, Ganopolski A, Kubatzki K, Petoukhov V (2003) Stability analysis of the climate-vegetation system in the northern high latitudes. Clim Change 57:119–138

Calov R, Ganopolski A, Petoukhov V, Claussen M, Greve R (2002) Large-scale instabilities of the Laurentide ice sheet simulated in a fully coupled climate-system model. Geophys Res Lett 29:2216

Campin J-M, Goosse H (1999) Parameterization of density-driven downsloping flow for a coarse-resolution ocean model in z-coordinate. Tellus 51A:412–430

CAPE project members (2001) Holocene paleoclimate data from the Arctic: testing models of global climate change. Quat Sci Rev 20:1275–1287

Claussen M, Kubatzki C, Brovkin V, Ganopolski A, Hoelzmann P, Pachur HJ (1999) Simulation of an abrupt change in Saharan vegetation in the mid-Holocene. Geophys Res Lett 26:2037–2040

Claussen M, Mysak LA, Weaver AJ, Crucifix M, Fichefet T, Loutre MF, Alexeev VA, Berger A, Ganopolski A, Goosse H, Lohmann G, Lunkeit F, Mohkov F, Petoukhov V, Stone P, Wang Z, Weber SL (2002) Earth System models of intermediate complexity: closing the gap in the spectrum of climate system models. Clim Dyn 18:579–586

Cramer W, Bondeau A, Woodward FI, Prentice IC, Betts RA, Brovkin V, Cox PM, Fisher V, Foley JA, Friend AD, Kucharik C, Lomas MR, Ramankutty N, Sitch S, Smith B, White A, Young-Molling C (2001) Global response of terrestrial ecosystem structure and function to CO2 and climate change: results from six dynamic global vegetation models. Glob Change Biol 7:357–373

Crucifix M, Loutre MF, Tulkens P, Fichefet T, Berger A (2002) Climate evolution during the Holocene: a study with an Earth system model of intermediate complexity. Clim Dyn 19:43–60

Cubasch U, Meehl GA, Boer GJ, Stouffer RJ, Dix M, Noda A, Senior CA, Raper S, Yap KS (2001) Projections of future climate change. In: Houghton JT, Ding Y, Griggs DJ, Noguer M, van der Linden PJ, Dai X, Maskell K, Johnson CA (eds) Climate change 2001: the scientific basis. Contribution of working group I to the third assessment report of the intergovernmental panel on climate change. Cambridge University Press, Cambridge, pp 525–582

Dahl SO, Nesje A (1996) A new approach to calculating Holocene winter precipitation by combining glacier equilibrium-line altitudes and pine-tree limits: a case study from Hardangerjøkulen, central southern Norway. Holocene 6:381–398

Deleersnijder E, Campin JM (1995) On the computation of the barotropic mode of a free-surface world ocean model. Ann Geophys 13:675–688

Duplessy JC, Ivanova E, Murdmaa I, Paterne M, Labeyrie L (2001) Holocene Paleoceanography of the northern Barents Sea and variations in the northward heat transport by the Atlantic Ocean. Boreas 30:2–16

Dyke AS, Savelle JM (2000) Holocene driftwood incursion to Southwestern Victoria Island, Canadian Arctic Archipelago, and its significance to Paleooceanography and Archaeology. Quat Res 54:113–120

Dyke AS, Savelle JM (2001) Holocene history of the Bering Sea Bowhead Whale (Balaena mysticetus) in its Beaufort Sea summer grounds off Southwestern Victoria Island, western Canadian Arctic. Quat Res 55:371–379

Fichefet T, Morales Maqueda MA (1997) Sensitivity of a global sea ice model to the treatment of ice thermodynamics and dynamics. J Geophys Res 102:12609–12646

Foley JA, Kutzbach JE, Coe MT, Levis S (1994) Feedbacks between climate and boreal forests during the Holocene epoch. Nature 371:52–54

Folland CK, Karl TR, Christy RA, Clarke RA, Gruza GV, Jouzel J, Oerlemans J, Salinger MJ, Wang S-W (2001) Observed climate variability and change. In: Houghton JT, Ding Y, Griggs DJ, Noguer M, van der Linden PJ, Dai X, Maskell K, Johnson CA (eds) Climate change 2001: the scientific basis. Contribution of working group I to the third assessment report of the intergovernmental panel on climate change. Cambridge University Press, Cambridge, pp 99–181

Gajewski K, Frappier M (2001) A Holocene lacustrine record of environmental change in northeastern Prince of Wales Island, Nunavut, Canada. Boreas 30:285–289

Ganopolski A, Kubatzki C, Claussen M, Brovkin V, Petoukhov V (1998) The influence of vegetation-atmosphere-ocean interaction on climate during the Mid-Holocene. Science 280:1916–1919

Gent PR, McWilliams JC (1990) Isopycnal mixing in ocean general circulation models. J Phys Oceanogr 20:150–155

Goosse H, Fichefet T (1999) Importance of ice-ocean interactions for the global ocean circulation: a model study. J Geophys Res 104:23337–23355

Goosse H, Renssen H (2001) A two-phase response of the Southern Ocean to an increase in greenhouse gas concentrations. Geophys Res Lett 28:3469–3472

Goosse, H, Renssen H (2003) Simulating the evolution of the Arctic climate during the last millennium. In: Proceedings of 7th conference on polar meteorology and oceanography and joint symposium on high-latitude climate variations, American Meteorological Society, Hyannis, 12–16 May 2003, Extended Abstract 1.5, at http://ams.confex.com/ams/7POLAR/7POLARCLIM/abstracts/60763.htm

Goosse H, Renssen H (2004) Exciting natural modes of variability by solar and volcanic forcing: idealized and realistic experiments. Clim Dyn 23:153–163

Goosse H, Deleersnijder E, Fichefet T, England M (1999) Sensitivity of a global ocean-sea ice model to the parameterization of vertical mixing. J Geophys Res 104:13681–13695

Goosse H, Selten FM, Haarsma RJ, Opsteegh JD (2001) Decadal variability in high northern latitudes as simulated by an intermediate-complexity climate model. Annals Glaciol 33:525–532

Goosse H, Selten FM, Haarsma RJ, Opsteegh JD (2002a) A mechanism of decadal variability of the sea ice volume of the Northern Hemisphere. Clim Dyn 19:61–83

Goosse H, Renssen H, Selten FM, Haarsma RJ, Opsteegh JD (2002b) Potential causes of abrupt climate events: a numerical study with a three-dimensional climate model. Geophys Res Lett 29:1860. DOI:10.1029/2002GL014993

Goosse H, Selten FM, Haarsma RJ, Opsteegh JD (2003) Large sea-ice volume anomalies simulated in a coupled climate model. Clim Dyn 20:523–536

Goosse H, Masson-Delmotte V, Renssen H, Delmotte M, Fichefet T, Morgan V, van Ommen T, Khim BK, Stenni B (2004) A late medieval warm period in the Southern Ocean as a delayed response to external forcing? Geophys Res Lett 31:L06203. DOI: 10.1029/019140

Hammarlund D, Barnekow L, Birks HJB, Buchardt B, Edwards TWD (2002) Holocene changes in atmospheric circulation recorded in the oxygen-isotope stratigraphy of lacustrine carbonates from northern Sweden. Holocene 12:339–351

Harington CR (1975) A postglacial walrus (Odobenus rosmarus) from Bathurst Island, N.W.T. Can Field Nat 89:249–261

Harvey LDD (1988) On the role of high latitude ice, snow and vegetation feedbacks in the climatic response to external forcing changes. Clim Change 13:191–224

Hewitt CD Mitchell JFB (1998) A fully coupled GCM simulation of the climate of the mid-Holocene. Geophys Res Lett 25:361–364

Hillaire-Marcel C, deVernal A, Bilodeau G, Weaver AJ (2001) Absence of deep-water formation in the Labrador Sea during the last interglacial period. Nature 410:1073–1077

Holland MM, Bitz CM (2003) Polar amplification of climate change in coupled models. Clim Dyn 21:221–232

Johnsen SJ, Dahl-Jensen D, Gundestrup N, Steffensen JP, Clausen HB, Miller H, Masson-Delmotte V, Sveinbjörnsdottir AE, White J (2001) Oxygen isotope and palaeotemperature records from six Greenland ice-core stations: Camp Century, Dye-3, GRIP, GISP2, Renland and NorthGRIP. J Quat Sci 16:299–307

Kaplan MR, Wolfe AP, Miller GH (2002) Holocene environmental variability in Southern Greenland inferred from Lake Sediments. Quat Res 58:149–159

Kaufman DS, Ager TA, Anderson NJ, Anderson PM, Andrews JT, Bartlein PJ, Brubaker LB, Coats LL, Cwynar LC, Duvall ML, Dyke AS, Edwards ME, Eisner WR, Gajewski K, Geirsdottir A, Hu FS, Kaufman DS, Ager TA, Anderson NJ, Anderson PM, Andrews JT, Bartlein PJ, Brubaker LB, Coats LL, Cwynar LC, Duvall ML, Dyke AS, Edwards ME, Eisner WR, Gajewski K, Geirsdottir A, Hu FS, Jennings AE, Kaplan MR, Kerwin MW, Lozhkin AV, MacDonald GM, Miller GH, Mock CJ, Oswald WW, Otto-Bliesner BL, Porinchu DF, Rühland K, Smol JP, Steig EJ, Wolfe BB (2004) Holocene thermal maximum in the western Arctic (0–180°W). Quat Sci Rev 23:529–560

Kerwin MW, Overpeck JT, Webb RS, DeVernal A, Rind DH, Healy RJ (1999) The role of oceanic forcing in mid-Holocene Northern Hemisphere climatic changes. Paleoceanography 14:200–210

Koç N, Jansen E, Haflidason H (1993) Paleoceanographic reconstructions of surface ocean conditions in the Greenland, Iceland and Norwegian Seas through the last 14 ka based on diatoms. Quat Sci Rev 12:115–140

Koç N, Jansen E (1994) Response of the high-latitude Northern Hemisphere to orbital climate forcing: evidence from the Nordic Seas. Geology 22:523–526

Koç, N, Jansen E, Hald M, Labeyrie L (1996) Late glacial-Holocene sea surface temperatures and gradients between the North Atlantic and the Norwegian Sea: implications for the Nordic heat pump. In: Andrews JT, Austin WEN, Bergsten H, Jennings AE (eds) Late quarternary palaeoceanography of the North Atlantic Margins, Geological Society Special Publication, vol 111. Geological Society, London, pp 177–185

Koerner RM, Fisher DA (1990) A record of Holocene summer climate from a Canadian high-Arctic ice core. Nature 343:630–631

Korhola A, Weckström J, Holmström L, Erästö P (2000) A quantitative Holocene climatic record from diatoms in Northern Fennoscandia. Quat Res 54:284–294

Kutzbach JE, Gallimore RG (1988) Sensitivity of a coupled atmosphere/mixed ocean model to changes in orbital forcing at 9000 years B.P. J Geophys Res 93:803–821

Lauritzen SE, Lundberg J (1999) Calibration of the speleothem delta function: an absolute temperature record for the Holocene in northern Norway. Holocene 9:659–669

Levac E, de Vernal A, Blake W Jr (2001) Sea-surface conditions in northernmost Baffin Bay during the Holocene: palynological evidence. J Quat Sci 16:353–363

Licciardi JM, Clark PU, Jenson JW, Macayeal DR (1998) Deglaciation of a soft-bedded Laurentide Ice Sheet. Quat Sci Rev 17:427–448

Lubinski DJ, Forman SL, Miller GH (1999) Holocene glacier and climate fluctuations on Franz Josef Land, Arctic Russia, 80°N. Quat Sci Rev 18:85–108

MacDonald GM, Edwards TWD, Moser KA, Pienitz R, Smol JP (1993) Rapid response of treeline vegetation and lakes to past climate warming. Nature 361:243–246

MacDonald GM, Velichko AA, Kremenetski CV, Borisova OK, Goleva AA, Andreev AA, Cwynar LC, Riding RT, Forman SL, Edwards TWD, Aravena R, Hammarlund D, Szeics JM, Gattaulin VN (2000). Holocene treeline history and climate change across Northern Eurasia. Quat Res 53:302–311

Marchal O, Cacho I, Stocker TF, Grimalt JO, Cavo E, Martrat B, Shackleton N, Vautravers M, Cortijo E, Van Kreveld S, Anderson C, Koç N, Chapman M, Sbaffi L, Duplessy JC, Sarnthein M, Turon JL, Duprat J, Jansen E (2002) Apparent long-term cooling of the sea surface in the northeast Atlantic and Mediterranean during the Holocene. Quat Sci Rev 21:455–483

Mellor GL, Yamada T (1982) Development of a turbulence closure model for geophysical fluid problems. Rev Geophys Space Phys 20:851–875

Mitchell JFB, Grahame NS, Needham KJ (1988) Climate simulations for 9000 years before present: seasonal variations and effects of the Laurentide Ice Sheet. J Geophys Res 93:8283–8303

Mitchell JFB, Karoly DJ, Hegerl GC, Zwiers FW, Allen MR, Marengo J (2001) Detection of climate change and attribution of causes. In: Houghton JT, Ding Y, Griggs DJ, Noguer M, van der Linden PJ, Dai X, Maskell K, Johnson CA (eds) Climate change 2001: the scientific basis. Contribution of working group I to the third assessment report of the intergovernmental panel on climate change. Cambridge University Press, Cambridge, pp 695–738

Naidina OD, Bauch HA (2001) A Holocene pollen record from the Laptev Sea shelf, northern Yakutia. Global Planet Change 31:141–153

Nesje A, Matthews JA, Dahl SO, Berrisford MS, Andersson C (2001) Holocene glacier fluctuations of Flatebreen and winter-precipitation changes in the Jostedalsbreen, western Norway, based on glaciolacustrine sediment records. Holocene 11:267–280

Opsteegh JD, Haarsma RJ, Selten FM, Kattenberg A (1998) ECBILT: a dynamic alternative to mixed boundary conditions in ocean models. Tellus 50A: 348–367

Ovenden L (1988) Holocene proxy-climate data from the Canadian Arctic. Paper 88-2. Geol Survey Canada, Ottawa

Peltier WR (1994) Ice age paleotopography. Science 265:195–201

Prentice IC, Jolly D, BIOME 6000 participants (2000) Mid-Holocene and glacial-maximum vegetation geography of the northern continents and Africa. J Biogeogr 27:507–519

Rahmstorf S, Marotzke J, Willebrand J (1996) Stability of the thermohaline circulation. In: Krauss W (ed) The warm water sphere of the North Atlantic Ocean. Borntraeger, Stuttgart, pp 129–158

Rasmussen TL, Bäckström D, Heinemeier J, Klitgaard-Kristensen D, Knutz PC, Kuijpers A, Lassen S, Thomsen E, Troelstra SR, van Weering TCE (2002) The Faroe-Shetland Gateway: Late Quaternary water mass exchange between the Nordic seas and the northeastern Atlantic. Marine Geol 188:165–192

Raynaud D, Barnola JM, Chappellaz J, Blunier T, Indermühle A, Stauffer B (2000) The ice record of greenhouse gases: a view in the context of future changes. Quat Sci Rev 19:9–17

Renssen H, Goosse H, Fichefet T, Campin J-M (2001) The 8.2 kyr BP event simulated by a global atmosphere–sea-ice–ocean model. Geophys Res Lett 28:567–570

Renssen H, Goosse H, Fichefet T (2002) Modeling the effect of freshwater pulses on the early Holocene climate: the influence of high frequency climate variability. Paleoceanography 17:1020. DOI: 10.1029/2001PA000649

Renssen H, Brovkin V, Fichefet T, Goosse H (2003a) Holocene climate instability during the termination of the African Humid Period. Geophys Res Lett 30:1184. DOI: 10.1029/2002GL016636

Renssen H, Goosse H, Fichefet T (2003b) On the non-linear response of the ocean thermohaline circulation to global deforestation. Geophys Res Lett 30:1061. DOI:10.1029/2002GL016155

Renssen H, Braconnot P, Tett SFB, von Storch H, Weber SL (2004) Recent developments in Holocene climate modelling. In: Battarbee RW, Gasse F, Stickley CE (eds) Past climate variability through Europe and Africa. Kluwer, Dordrecht, pp 495–513

Rossow WB, Walker AW, Beuschel DE, Roiter MD (1996) International satellite cloud climatology project (ISCCP) documentation of new cloud datasets. WMO/TD-No 737. World Meteorological Organisation, Geneva

Ritchie JC, Cwynar LC, Spear RW (1983) Evidence from northwest Canada for an early Holocene Milankovitch thermal maximum. Nature 305:126–128

Salvigsen O, Forman SL, Miller GH (1992) Thermophilous molluscs on Svalbard during the Holocene and their paleoclimatic implications. Polar Res 11:1–10

Seppä H, Hammarlund D (2000) Pollen-stratigraphical evidence of Holocene hydrological change in northern Fennoscandia supported by independent isotopic data. J Paleolimnol 24:69–79

Seppä H, Birks HJB (2001) July mean temperature and annual precipitation trends during the Holocene in the Fennoscandian tree-line area: pollen-based climate reconstructions. Holocene 11:527–539

Seppä H, Birks HJB (2002) Holocene climate reconstructions from the Fennoscandian tree-line area based on pollen data from Toskaljavri. Quat Res 57:191–199

Seppä H, Birks HH, Birks HJB (2002) Rapid changes during the Greenland stadial 1 (Younger Dryas) to early Holocene transition on the Norwegian Barents Sea coast. Boreas 31:215–225

Schaeffer M, Selten FM, Opsteegh JD, Goosse H (2002) Intrinsic limits to predictability of abrupt regional climate change in IPCC SRES scenarios. Geophys Res Lett 29:1767. DOI 10.1029/2002GL015254

Smith IR (2002) Diatom-based Holocene paleoenvironmental records from continental sites on northeastern Ellesmere Island, high Arctic, Canada. J Paleolimnol 27:9–28

Snyder JA, MacDonald GM, Forman SL, Tarasov GA, Mode WN (2000) Postglacial climate and vegetation history, north-central Kola Peninsula, Russia: pollen and diatom records from Lake Yarnyshnoe-3. Boreas 29:261–271

Solignac S, de Vernal A, Hillaire-Marcel C (2004) Holocene sea-surface conditions in the North Atlantic—contrasted trends and regimes in the western and eastern sectors (Labrador Sea vs. Iceland Basin). Quat Sci Rev 23:319–334

Stewart TG, England J (1983) Holocene sea-ice variations and paleoenvironmental change, northernmost Ellesmere Island, N.W.T. Canada. Arctic Alpine Res 15:1–17

Stewart TG, England J (1986) An early Holocene Caribou antler from northern Ellesmere Island, Canadian Arctic archipelago. Boreas 15:25–31

Stott PA, Tett SFB, Jones GS, Allen MR, Mitchell JFB, Jenkins GJ (2000) External control of twentieth century temperature variations by natural and anthropogenic forcings. Science 290:2133–2137

TEMPO members (1996) Potential role of vegetation feedback in the climate sensitivity of high-latitude regions: a case study at 6000 years BP. Global Biochem Cycle 10:727–736

Thompson DW, Wallace JM (1998) The Arctic Oscillation signature in the wintertime geopotential height and temperature fields. Geophys Res Lett 25:1297–1300

Tuenter E, Weber SL, Hilgen FJ, Lourens LJ (2004) The influence of precession and obliquity on the Atlantic/European winter climate. In: Tuenter E, Modeling orbital induced variations in circum-Mediterranean climate. PhD Thesis, Utrecht University

Vardy SR, Warner BG, Aravena R (1998) Holocene climate and development of a subarctic peatland near Inuvik, Northwest Territories, Canada. Clim Change 40:285–313

Voronina E, Polyak L, De Vernal A, Peyron O (2001) Holocene variations of sea-surface conditions in the southeastern Barents Sea, reconstructed from dinoflagellate cyst assemblages. J Quat Sci 16:717–726

Wang Y, Mysak L, Wang Z, Brovkin V (2004) The greening of the McGill Paleoclimate model. Part II: Millennial-scale climate changes. Clim Dyn (submitted)

Weber SL (2001) The impact of orbital forcing on the climate of an intermediate-complexity coupled model. Global Planet Change 30:7–12

Weber SL, Oerlemans J (2003) Holocene glacier variability: three case studies using an intermediate complexity climate model. Holocene 13:353–363

Weber SL, Crowley TJ, van der Schrier G (2004) Solar irradiance forcing of centennial climate variability during the Holocene. Clim Dyn 24:539–553

Werner M, Mikolajewicz U, Heimann M, Hoffmann G (2000) Borehole versus isotope temperatures on Greenland: seasonality does matter. Geophys Res Lett 27:723–726

Williams LD, Bradley RS (1985) Paleoclimatology of the Baffin Bay region. In: Andrews JT (ed) Quaternary environments: eastern Canadian Arctic, Baffin Bay and Western Greenland. Allen and Unwin, Boston, pp 741–772